7-12-2021

Laboratory and full-scale pavement sections testing for evaluating frost action in cold regions

Dorin Papuc
Rowan University

LABORATORY AND FULL-SCALE PAVEMENT SECTIONS TESTING FOR EVALUATING FROST ACTION IN COLD REGIONS

by

Dorin Papuc

A Thesis

Submitted to the
Department of Civil and Environmental Engineering
College of Engineering
In partial fulfillment of the requirement
For the degree of
Master of Science in Civil Engineering
at
Rowan University
June 30, 2021

Thesis Chair: Yusuf Mehta, Ph.D., P.E.

Committee Members:
Cheng Zhu, Ph.D.
Gilson Lomboy, Ph.D.

Abstract

Dorin Papuc
LABORATORY AND FULL-SCALE PAVEMENT SECTIONS TESTING FOR EVALUATING FROST ACTION IN COLD REGIONS
2018-2021
Yusuf Mehta, Ph.D., P.E.
Master of Science in Civil Engineering

A comprehensive laboratory testing plan was conducted as part of this project to select two frost-susceptible soils for use in constructing three full-scale test strips. A total of 16 soils were obtained from various suppliers in NJ and were evaluated to determine their frost-susceptibility. The evaluation included conducting sieve analysis, hydrometer analysis, and specific gravity. Using these measures, two soils were selected (namely, Soil #2 and Soil #13) for constructing the test strips. The properties (Atterberg Limits, moisture-density relationships, California bearing ratio (CBR), Resilient Modulus among others) were determined through a laboratory testing plan. In addition, this study involved constructing three full-scale test strips (as one section) at the CREATEs full-scale testing facility. The first test strip was constructed using a typical NJ HMA mix, a typical dense graded aggregate base (DGA), and Soil #2 used as the subgrade. Test Strip II was constructed using the same HMA mix, a blend of DGA and Soil #13 (one to one), and Soil #2 as the subgrade layer. Test Strip III had a blend of DGA and Soil #13 for the base layer and a one-to-one blend of Soils #2 and #13 for the subgrade layer. All three test strips were evaluated using the HWD on weekly basis. Test Strip I also included a thermal conductivity probe that is capable of measuring moisture content, temperature, and thermal conductivity at varying depths in the base and subgrade layers.

Table of Contents

Abstract iii

List of Figures viii

List of Tables xi

Chapter 1: Introduction 1

Background 1

Problem Statement 2

Research Hypothesis 3

Significance of Study 3

Goal & Objectives 4

Document Outline 5

Chapter 2: Literature Review 6

Pavement's Exposure to Freeze-Thaw Cycling 6

Freezing of Pavement Structure and Frost-Heave Formation 7

Seasonal Variations' Effects on Resilient Modulus of Unbound Layers 9

Characterization of Frost-Susceptible Soils 11

USACE Particle Size Criteria for Frost-Susceptible Soils 13

Frost-Depth Prediction Theories and Models 17

ModBerg Equation 17

FROST Model 18

Frost-Depth Predictions in Real-Life Conditions 20

Table of Contents (Continued)

Summary of Literature Review 24

Chapter 3: Materials and Laboratory Experimental Program 26

Materials Evaluated 26

Experimental Program 29

Specific Gravity 31

Particle-Size Analysis 31

Atterberg Limits 32

Standard Proctor Compaction Test 33

Strength Tests 35

Chapter 4: Laboratory Results Discussion 37

Atterberg Limits 37

Classification of Soils #2 and #13 38

Moisture-Density Relationships 40

California Bearing Ratio (CBR) 41

Resilient Modulus 42

Summary of Findings from Laboratory Testing 44

Chapter 5: Construction of Full-Scale Pavement Sections 46

Selection of Test Strips Location (Shadow Analysis) 46

Pavement Sections and Materials 49

Table of Contents (Continued)

Pavement Sections and Materials 50

Construction Activities 56

Surveying and Excavation 56

Insulation and Waterproofing 59

Aggregate Filter Layer and Permeable Fabric 60

Placement and Compaction of Subgrade Layers 61

Placement and Compaction of Base Layers 63

Placement and Compaction of Asphalt Layers 65

Drilling Holes for Sensor Probe and Saturation Pipes 69

Dynamic Cone Penetrometer (DCP) Testing and Results 70

Instrumentation of Test Strips 72

Thermal-Conductivity Sensors 72

Weather Station 73

Thermocouples for Measuring HMA Temperature 73

Plan for Heavy Weight Deflectometer (HWD) Testing and Monitoring of Sections 74

HWD Testing 74

Monitoring of Moisture, Thermal Conductivity, and Temperature of Test Strips 75

Chapter 6: Discussion of Field Testing Results 76

Temperature, Moisture, and Thermal Conductivity Variation 76

HWD Measured Deflections 82

Table of Contents (Continued)

Impact of Moisture and Temperature on Backcalculated Layer Moduli. 84

Chapter 7: Summary, Conclusions and Recommendations 90

Summary 90

Summary of Findings 91

Conclusions 93

Recommendations 96

References 98

List of Figures

Figure Page

Figure 1. Freezing Phenomenon and Heave Formation in a Pavement Structure. 9

Figure 2. Impact of Seasonal Variations on Pavement Structures (Washington State Department of Transportation, Report No. WA-RD 80.2). 11

Figure 3. Rates of Heave in Laboratory Freezing Tests (USACE, 1984)..... 17

Figure 4. Instrumentation Used for Evaluating the Bearing Capacity of New Jersey Soils at Rutgers University (K.A. Turner & A.R. Jumikis, 1956). 22

Figure 5. The Danish Road-Testing Machine (Zhang & McDonald, 2003)..... 23

Figure 6. Sieve Analysis Results of All Materials (Soils and Aggregates) Samples Collected. 28

Figure 7. Specific Gravity and Hydrometer Analysis Results for Soils #2, #13 and #16. 30

Figure 8. Liquid Limits (LL) for Soils #2 and #13. 37

Figure 9. Plastic Limit (PL) and Plasticity Index (PI) for Soils #2 and #13. 38

Figure 10. Moisture-Density Relationships for Soils #2 and #13. 40

Figure 11. California Bearing Ratio Values for Soils #2 and #13. 41

Figure 12. Average Measured Resilient Modulus Values for Soil #2. 43

Figure 13. Pictures of Pond Fill (ML) Soil Samples in the Conditioning Phase of Resilient Modulus Testing. 43

Figure 14. Sun Movement and Shadow on Sections Selected Location..... 47

Figure 15. Shadow Analysis for January 15th at different times of the day..... 48

Figure 16. Aerial Image of Test Strips Location. 49

Figure 17. Structure of the Pavement Test Strips. 51

Figure 18. Gradation and Optimum Binder Content of Asphalt Mix. 52

List of Figures (Continued)

Figure Page

Figure 19. Gradation and DGA and One to One Blend of DGA and Soil #13. 53

Figure 20. Blending of Soils Using a Bucket Loader. 54

Figure 21. Gradation of Soil #2 and Blend (Soils #2 and #13) Used as Subgrade Layers 55

Figure 22. Pictures of Making and Surveying of Section. 57

Figure 23. Pictures of Excavation Process and Depth Evaluation. 58

Figure 24. Insulation and Waterproofing of Section. 60

Figure 25. Aggregate Filter Layer and Permeable Fabric. 61

Figure 26. Placement and Compaction of Subgrade Layers in Each Test Strip. 62

Figure 27. Placement and Compaction of Base Layers in Each Test Strip. 64

Figure 28. Rain Accumulation and Covering of Section before Placement of HMA. 66

Figure 29. Placement and Compaction of HMA. 67

Figure 30. Nuclear Gauge Density Measurements. 68

Figure 31. Nuclear Gauge Measurements Locations and Averaged Density Values. 69

Figure 32. Drilling Holes for Sensors and Saturation Pipes. 69

Figure 33. DCP Testing of Test Strips. 71

Figure 34. Thermal-Conductivity Sensors. 72

Figure 35. ClimaVUE Weather Station. 73

Figure 36. Location of Embedded Thermocouples 74

Figure 37. Picture of HWD Used in This Study. 75

Figure 37. Picture of HWD Used in This Study. 75

List of Figures (Continued)

Figure Page

Figure 39. Variation of Temperature, Moisture Content, and Thermal Conductivity in Test Strip I (Values at Mid-Point of Layer). 80

Figure 40. Variation of Temperature, Moisture Content, and Thermal Conductivity with Depth. 81

Figure 41. Heavy Weight Deflectometer (HWD) Deflections Measured for Test Strip I. 86

Figure 42. Heavy Weight Deflectometer (HWD) Deflections Measured for Test Strip II. 87

Figure 43. Heavy Weight Deflectometer (HWD) Deflections Measured for Test Strip III 88

Figure 44. Variation of Back Calculated Stiffness with Time. 89

List of Tables

Table Page

Table 1. U.S. Army Corps of Engineers' Frost-Susceptibility Criteria (USACE, 1984) 14

Table 2. Description of USACE's F1 through F4 Frost-Susceptible Soils Groups (USACE, 1984) 16

Table 3. Locations in New Jersey from which Soils were Obtained 27

Table 4. Experimental Testing Program of Selected Soils 29

Table 5. Classification of Soils #2 and #13 Using the Unified Soils Classification System (USCS) 39

Table 6. Properties of Dense Aggregate (DGA) and Blended Base Layer Aggregate 53

Table 7. Classification of Soils #2 and #13 Using the Unified Soils Classification System (USCS) 56

Table 8. Control Measurements for Section's Excavation 59

Table 9. Subgrade Layer Nuclear Gauge Density Measurements 63

Table 10. Base Layer Nuclear Gauge Measurements 65

Table 11. Avearge Sand Cone Density Test Results 65

Table 12. HMA Layer Nuclear Gauge Measurements 68

Table 13. In-Situ Calculated CBR Values for Base and Subgrade Layers 71

Chapter 1

Introduction

Background

The design of pavement structures in cold and arctic regions necessitates specific considerations primarily because these regions are subjected to frost action. The U.S. Army Corps of Engineers developed a guideline to address the concerns associated with seasonal frost action (e.g., ice segregation) and its influence on pavement design procedures (USACE 1984). Pavement's structural capacity depends on the strength of materials used in pavement construction and layer thicknesses. While layer thicknesses essentially remain the same during design life, material strength may significantly vary. In common practices of pavement design, strength of materials is characterized by modulus, a mechanical property of the material. One important phenomenon that impacts modulus is freeze/thaw. Freeze/thaw cycles typically lead to seasonal variation of modulus, which will, in turn, adversely affect pavement's performance.

Knowing the effects of frost action and determining frost depth within pavement structures can help improve the existing guidelines and integrate them into pavement design procedures.

Various mechanistic, empirical, and mechanistic-empirical models were developed for predicting frost depth (Rajaei and Baladi 2015). The early prediction models were predominantly empirical and were based on the cumulative freezing index (CFI) parameter. The field studies showed that these equations overestimated the frost depth, thus, a correction factor was introduced by the modified Berggren (ModBerg)

equation to address this discrepancy. In reality, a variety of parameters are involved in the prediction of frost depth including soil type and gradation, moisture content, type of moisture (i.e., pore or adsorbed water), depth of ground water table (G.W.T.), existence of external water source (e.g., surface runoff), level of capillary support, and climatic conditions including air temperature, solar radiation, wind speed, precipitation, cloud ratio, and relative humidity. Therefore, it is critical to analyze frost/thaw action in pavements along with the above mentioned parameters, for a better understanding of frost/thaw phenomenon and a more precise frost depth determination. This will help improve the design of pavement structures and will lower the impact of deformations.

Problem Statement

Researchers have conducted extensive studies to analyze frost penetration and spring thawing in pavement structures. This has helped them in determining frost depth in pavements for decades. However, the prediction model used (ModBerg Model) has the following flaws:

- The surface temperature is considered to drop from annual mean air temperature to a value equal to averaged frost daily freezing index and remains constant during the entire freezing season (Bianchini and Gonzalez, 2012).
- Constant thermal properties (e.g., thermal conductivity, specific heat capacity, etc.) are assigned to the thawed or frozen soils, while in reality these parameters vary with temperature and moisture content.
- No boundary soils are considered, which are partially thawed and partially frozen soils.

Therefore, additional research should be conducted to study how frost penetration and spring thawing are taking place inside the pavement structures, along with the moisture and temperature transfer between the structure's layers. This will help determining frost depth with a higher precision, design pavement structures better so they can develop less deformations and also predict the maximum allowed load (traffic) on top of these structures during spring thaw periods, when roads are weaker.

This study was conducted to investigate how fluctuations in weather conditions (temperature, wind speed, solar radiation etc.) along with moisture flow and thermo-conductivity variations inside the layers of a pavement structure affect frost penetration inside pavements.

Research Hypothesis

This research was conducted to investigate the hypothesis that moisture and temperature variations within frost-susceptible layers affect the stiffness of a pavement structure. Temperature, moisture and thermal conductivity are factors that influence frost penetration within pavements with frost-susceptible layers. These factors can be considered to predict frost depth with a higher precision.

Significance of Study

This study was conducted to evaluate the impact of freeze/thaw cycles on pavement structures and determine how boundary soils and their properties (moisture and thermo-conductivity) affect frost action in pavement structures. The study is meant to replicate pavement structures from cold and arctic regions and provide information for the validation of FROST (Finite Response of Soils at all Temperatures) model, a new

frost depth prediction model developed by U.S. Army Corps of Engineers (USACE). If successful, the study will have the following benefits for Department of Defense (DoD):

- Help military engineers in designing cost-effective asphalt and rigid pavements;
- Longer lasting pavements based on sound engineering principals;
- Validate the updated frost depth calculations procedure;
- Validate the soils modulus prediction model used in pavement design.

Goal & Objectives

The goal of this study was to identify correlations between factors (type of material, moisture, temperature and thermal conductivity of layers) that affect frost action in pavements and to collect data for validating the FROST model developed by researchers at CRREL. To achieve this goal, three full-scale pavement sections were constructed at the Rowan University Accelerated Pavement Testing Facility (RUAPTF). The materials used for these strips (in subgrade and base layers) were specifically selected to be frost-susceptible. The specific goals of this full-scale testing study at Rowan University include:

- Select two frost-susceptible soils for use in full-scale construction of three tests strips;
- Characterize the properties of the two selected frost-susceptible soils;
- Construct three frost-susceptible full-scale pavement sections at RUAPTF;
- Install instrumentation in each of these test strips and monitor the changes in temperature, moisture content, and thermal conductivity as time progresses;

- Conduct Heavy Weight Deflectometer (HWD) test on all three test strips on weekly basis.

Document Outline

This document is divided into seven chapters. The first chapter provides a brief introduction and goals of the project. Chapter two presents a summary of literature pertaining to the impact of freeze-thaw cycling on pavement structures, the definition of frost-susceptible soils, frost depth prediction models, and more. Chapter three presents a discussion of materials used for this study along with the experimental plans for selecting two frost susceptible soils for use in the construction of three test strips. Chapter four offers a discussion of the laboratory testing results conducted on the selected frost susceptible soils. In Chapter five, a discussion of construction activities and pavement structure of each strip is presented. Chapter six presents a discussion of the field testing of the sections and analysis of collected sensor data. Chapter seven presents a summary of findings and conclusions drawn.

Chapter 2

Literature Review

Pavement's Exposure to Freeze-Thaw Cycling

The design and construction of pavement structures in cold regions must follow specific criteria and procedures, as these pavements, besides the common distresses, are subjected to frost heave action, as well as extreme changes in load-carrying capacity of subgrade and base layers. The impact of freezing conditions on pavement structure is manifested by heave formation during winter and loss of strength of base and subgrade soils during spring, when ice thawing takes place. Freezing weather conditions also impact pavements in other ways, causing the development of permanent roughness and excessive cracking. These in turn lead to excessive maintenance and the need for pavement rehabilitation/reconstruction. In order to account for all these negative effects, the U.S. Army Corps of Engineers developed a guide-line and integrated it into the pavement design procedure for cold regions (USACE, 1984).

A pavement structure exposed to freeze-thaw cycles experiences significant changes in its mechanical properties due to variations in temperature and moisture content. Soil (or unbound) layers become stiffer once the water entrapped in them freezes and ice lenses form; thus, increasing the pavement's bearing capacity. Despite the stiffening effect of freezing unbound layers, freezing action also causes differential heave in the upper layers (hot mix asphalt, HMA) leading to severe cracking. Pavements exposed to frost action are also subjected to a large amount of deterioration during spring, when ice thaw takes place and the pavement loses its bearing capacity as result of water

saturation of the layers. The large amount of moisture inside unbound pavement layers reduces the friction between soil particles. When the water drains out of these layers, excessive settlements occur; exposing the upper layers to high deformation levels.

The phenomenon of frost penetration can occur in two different ways: shallow frost penetration which takes place during warmer winters with higher temperatures. The second is deep frost penetration occurring during severe winters with subfreezing temperatures. Shallow frost penetration has a more pronounced negative impacts on pavements, than deep penetration, because it causes the formation of more ice lenses closer to a pavement's surface. This also results in a large amount of water in upper unbound layers when these ice lenses melt in spring. In contrast to shallow frost penetration, deep frost penetration is a slower process that takes places over a long period of time.

Freezing of Pavement Structure and Frost-Heave Formation

As mentioned above, freezing temperatures will cause frost heave formation and thawing will cause unbound pavement layers to lose their load-carrying capacity. Frost heave occurs when water within unbound pavement layers freezes and expands in volume. This expansion in volume is the main cause for frost heave. The amount of free water that contributes to ice formation is directly proportional to heave size. In general, the formation of ice lenses begins at the boundaries between pavement layers. The thickness of ice lenses is determined by the amount of circulating water within a soil layer and heat transfer between the layers. Usually, slow frost penetration will cause a small number of thick ice lenses to form, while a sudden freeze will develop a large

number of smaller and thinner ice lenses. Three conditions are generally needed to for frost heave to occur in pavement structures. These include: 1) presence of cold (subfreezing) weather penetrating the pavement; 2) adequate water source close enough to the pavement' surface or within the unbound layers, and 3) presence of frost-susceptible layers (soils) capable of holding moisture, typically with capillary support.

Figure 1 presents the phenomenon for frost heave formation in a pavement structure. As shown in this figure, cold weather penetrates down into the pavement layers. The freezing depth depends on different parameters including air temperature, duration of the cold season and thermal properties of the pavement layers, specifically, thermal diffusivity. The existence of ground water table (G.W.T.) is another condition required for soil freezing to occur. Theoretically, ground water will saturate the layers underneath it. However, if the G.W.T. is located within a frost-susceptible layer, it may potentially saturate (fully or partially) the dry areas of the same layer, as well as the above layers it due to capillary rise. Areas closer to G.W.T. are anticipated to experience higher saturation levels, while areas closer to pavement surface may be partially saturated or not saturated at all. Typically, for areas above G.W.T., the closer the distance to G.W.T., the higher the saturation level will be. The capillary rise depends on many parameters, among which, material type, porosity and gradation are the most important parameters (Johnson, 2012). While the existence of cold weather penetrating the pavement structure and the existence of ground water are required for the freezing process to happen, the freezing weather penetrating the pavement must get into the areas affected by the capillary effect in order to form ice lenses, process known as ice segregation. If the cold weather penetration depth and capillary rise both happen, but the

subsurface temperature of areas saturated due to capillary rise is above the freezing point, then freezing does not occur. Conversely, if the depth freezing and capillary rise overlap, freezing will happen and ice lenses will form in the overlapped areas. Figure 1 presents the freezing areas and how the ice lenses are formed. The size of ice lenses may vary depending on the distance from G.W.T. and on the saturation level.

Figure 1

Freezing Phenomenon and Heave Formation in a Pavement Structure

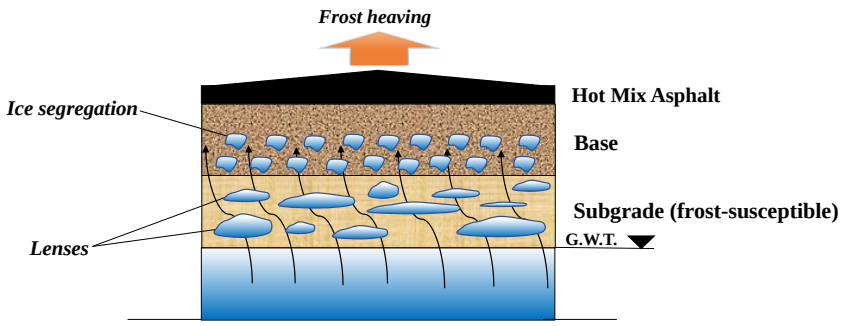

Seasonal Variations' Effects on Resilient Modulus of Unbound Layers

The structural capacity of pavements depends on the strength of the materials and layer thicknesses as well as on layer interface boundary conditions. While layer thicknesses and interface conditions essentially remain the same during the design life of a pavement structure, the strength of materials may significantly vary, due to moisture and temperature fluctuations. In common pavement design practices, the strength of materials in unbound layers is characterized by resilient modulus (a mechanical property of soils). Resilient modulus changes within unbound layers due to freeze-thaw cycling (when water is present). Freeze-thaw cycling typically lead to seasonal variations in unbound layer moduli values; adversely affect pavement performance and service life.

Freezing causes the modulus of affected layer(s) to artificially increase as a result of air voids being replaced with ice lenses. The resilient modulus values can rise during winter up to 20–120 times higher than the normal unfrozen conditions (Popik and Olidis, 2005). Although, freezing will increase a pavement's bearing capacity, there are other issues that adversely affect its performance. For example, formation of ice lenses will cause frost heave (as discussed previously) leading to cracking and higher surface roughness (Johnson, 1974).

In spring, ambient temperatures increase, causing ice lenses to thaw and shrink in volume. This consequently leads to formation of weak areas. Saturated unbound layers close to the surface of the pavement will be weak after thawing due to reduced shear strength. This is the case because melting of ice lenses starts from the areas closer to pavement surface. This, coupled with low downward drainage of water creates these weak areas in the upper unbound layers (Lambe, 1956). These weak areas will increase the potential of settlement (when water drains out eventually) and result in lower modulus (or bearing capacity), and failure of base and HMA layers in many instances.

Pavement deterioration caused by spring thaw differs from one pavement system to another. It is impacted by multiple factors such as: type and condition of the subgrade, temperature, amount of precipitation, traffic and frost-susceptibility of the soils. The time needed for a pavement to recover from thaw weakening is influenced by frost penetration depth, soil type and the drainage system. If the pavement is too weak, traffic or load restrictions can be applied, until the pavement structure recovers its load carrying capacity.

Figure 2 presents the seasonal variation of pavement deflection during a year for a portion of State Route 172 in Washington State (Mahoney, 1986). As can be seen in this figure, pavement deformations decrease in winter due to freezing of unbound layers. However, these deformations increase significantly during the spring thaw period. From Figure 2, it can be seen that freeze-thaw cycling directly impacts pavements' performance; thus, it is essential to understand this phenomenon.

Figure 2

Impact of Seasonal Variations on Pavement Structures (Washington State Department of Transportation, Report No. WA-RD 80.2)

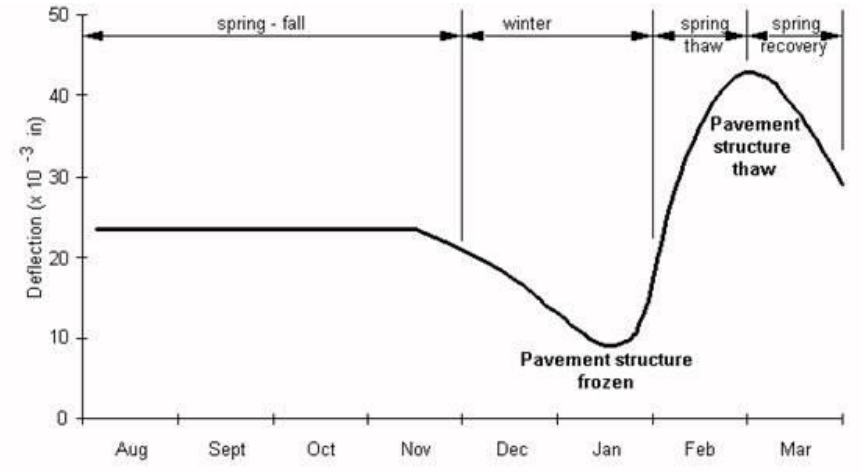

Characterization of Frost-Susceptible Soils

Frost action is more prevalent in pavements with frost-susceptible layers (usually the natural subgrade). The U.S. Army Corps of Engineers defines a frost-susceptible soil as "soil in which significant detrimental ice segregation will occur when the requisite moisture and freezing conditions are present." (USACE, 1984). Non-frost-susceptible

soils are also defined as “materials with non-detrimental ice segregation under naturally freezing conditions”.

To characterize the properties of frost susceptible soils, two main methods and definitions exist. The first is established by Casagrande (1931). According to Casagrande (1931), non-uniform soils containing at least 3 percent of particles finer than 0.02 mm and uniform soils containing at least 10 percent finer than 0.02 mm are defined as frost-susceptible. That is, considerable ice segregation is expected in these soils under naturally occurring freezing conditions and enough water supply (Casagrande, 1931). Therefore, the percentage of fine particles in a soil is recognized as major property for characterizing frost-susceptibility. In the field, a granular soil that is not frost-susceptible, may become frost-susceptible. This is possible when fine particles from lower layers (usually the subgrade) migrate to the upper granular base or subbase layers (Rajaei and Baladi, 2015).

The second approach for characterizing the properties of frost-susceptible soils is that of the U.S. Army Corps of Engineers (USACE, 1984). In this method, soils containing a portion of particles smaller than 0.02 mm (additional details provided in the following subsection) are generally identified as frost-susceptible (USACE, 1984). This method of classification based on fine particles works for soils with small amounts of fines, but not for soils with intermediate percentages (15-25%) of fines (Edgers, 1988). Soils with intermediate percentages of fines may show a well or poor frost performance, with scattered test results.

Despite the simplicity of fine particle criteria, these classification methods are not reliable and need to be complemented with other tests such as hydrometer and Atterberg

limits. Performing one or more of these additional tests will contribute to a better understanding of frost-susceptibility. Even with these tests, it is still important to note that uncertainty associated with classifying soils as frost-susceptible still exists because correlations between supplementary tests (e.g., Atterberg limits) and frost-susceptibility are not well-established (Konrad, 1999).

USACE Particle Size Criteria for Frost-Susceptible Soils

One of the soil characteristics affecting frost action is particle size. The particle size criterion is typically defined as a percentage of fine particles smaller than 0.075 mm. Additional testing (Atterberg limits) is also required to further define frost susceptibility. The U.S. Army Corps of Engineers considers soils as frost susceptible to some degree, if the soils have a portion of the particles smaller than 0.02mm (USACE, 1984).

The U.S. Army Corps of Engineers classifies the soils into two main categories: possibly frost-susceptible (PFS) and non-frost-susceptible (NFS) (USACE, 1984). Soils classified as PFS are further tested (Atterberg limits) to define their frost-susceptibility. Table 1 presents the U.S. Army Corps of Engineers' particle size criteria for classifying soils as NFS or PFS (USACE, 1984). As shown in this table, soils are grouped into eight different groups for frost design purposes. The first four groups are used as base and subbase layers. It is also noted that the subgroups under F3 and F4 are not arranged in the order of frost-susceptibility potential. There is some overlapping in frost susceptibility between these groups, with soils from group F4 having very high frost susceptibility.

Table 1

U.S. Army Corps of Engineers' Frost-Susceptibility Criteria (USACE, 1984)

Frost group		Kind of soil	Percentage finer than 0.02 mm by weight	Typical soil types under the Unified Soil Classification System
NFS*	(a)	Gravels	0.0–1.5	GW, GP
		Crushed stone		
		Crushed rock		
	(b)	Sands	0.0–3.0	SW, SP
PFS**	(a)	Gravels	1.5–3.0	GW, GP
		Crushed stone		
		Crushed rock		
	(b)	Sands	3.0–10.0	SW, SP
S1		Gravelly soils	3.0–6.0	GW, GP, GW-GM, GP-GM
S2		Sandy soils	3.0–6.0	SW, SP, SW-SM, SP-SM
F1		Gravelly soils	6.0–10.0	GM, GW-GM, GP-GM
F2	(a)	Gravelly soils	10.0–20.0	GM, GW-GM, GP-GM
	(b)	Sands	6.0–15.0	SM, SW-SM, SP-SM
F3	(a)	Gravelly soils	Over 20.0	GM, GC
	(b)	Sands, except very fine silty sands	Over 15.0	SM, SC
	(c)	Clays, PI less than 12	--	CL, CH
F4	(a)	All silts	--	ML, MH
	(b)	Very fine silty	Over 15	SM
	(c)	Clays, PI greater than 12	--	CL, CL-ML
	(d)	Varved clays and other fine-grained, banded sediments	--	CL and ML; CL, ML, and SM; CL, CH, ML, and SM

* Non-frost-susceptible.

** Possibly frost-susceptible but requires laboratory testing to determine frost design soil classification

The gravelly soils group (S1) have very low to medium frost susceptibility and can be used as subbase course. These soils will manifest less frost heave and higher resistance to freeze-thaw cycles comparing to F1 soils.

Soils falling in the S2 group (sandy soils) have very low to medium frost susceptibility and are suitable for subbase courses. Compared to F2 soils group, S2 soils have a lower number of particles finer than 0.02 mm and generally manifest less frost heave and higher strength after spring thaw (USACE, 1984). The difference between S1 and S2, is that S1 groups are “gravelly” soils whereas S2 are “sandy” soils.

The F1 group of soils includes frost susceptible gravelly soils, with a higher bearing capacity during spring thaw than F2 soils. However, Both, F1 and F2 soils experience equal ice segregation. A summary description of soil types F1 through F4 is presented in Table 2. Figure 3 presents a qualitative scale for frost-susceptibility of various soil types (USACE, 1984). While heave rate under normal freezing field conditions is typically 0.1 to 1.0 inch/day, the values presented in Figure 3 are greater, as laboratory tests are more conservative.

Table 2

Description of USACE's F1 through F4 Frost-Susceptible Soils Groups (USACE, 1984)

Group	Description
F1	Gravelly soils containing between 3 and 10 percent finer than 0.02 mm by weight.
F2	(a) Gravelly soils containing between 10 and 20 percent finer than 0.02 mm by weight (b) sands containing between 3 and 15 percent finer than 0.02 mm by weight.
F3	(a) Gravelly soils containing more than 20 percent finer Than 0.02 mm by weight (b) sands, except very fine silty sands, containing more than 15 percent finer than 0,02 mm by weight (c) clays with plasticity indexes of more than 12.
F4	(a) All silts (b) very fine silty sands containing more than 15 percent finer than 0.02 mm by weight (c) clays with plasticity indexes of less than 12 (d) varved clays and other fine-grained banded sediments.

Figure 3

Rates of Heave in Laboratory Freezing Tests (USACE, 1984)

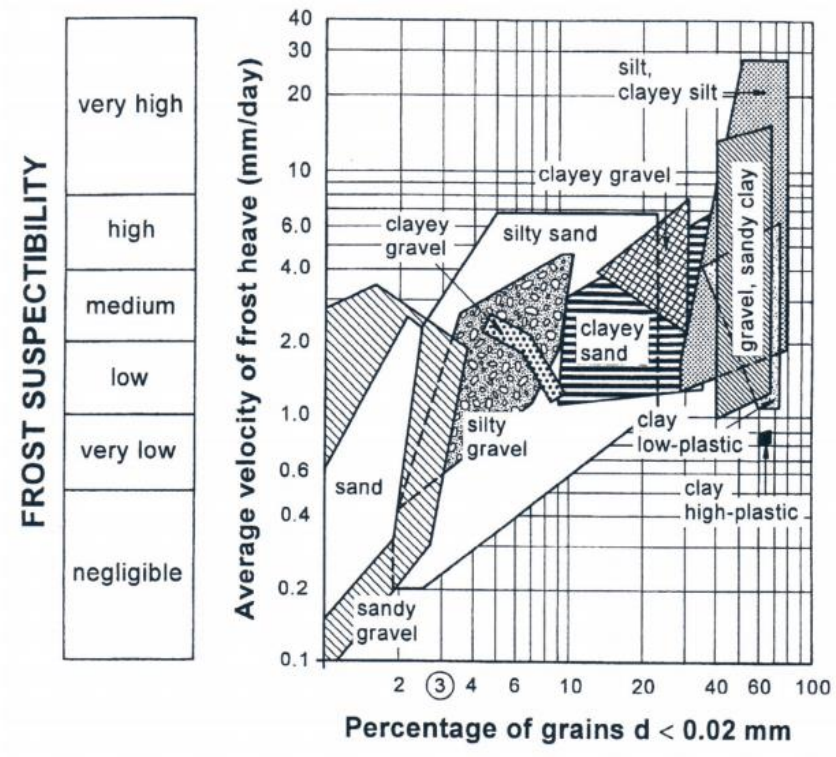

Frost-Depth Prediction Theories and Models

ModBerg Equation

ModBerg (Modified Berggren Equation) is an equation used to predict frost depth in soils. ModBerg was created by Aldrich (Rajaei and Baladi, 2015) by adding the coefficient λ to the existing Berggren Equation. This correction factor accounts for the effects of temperature changes in soil.

ModBerg equation is based on the Cumulative Freezing Index (CFI) and the average thermal conductivity value k_{avg} (Andersland and Ladanyi, 2004):

$$P = \lambda \sqrt{\frac{48 k_{avg} * n * CFI}{L}},$$

Where: P=frost depth, λ=correction factor, k_{avg}=average thermal conductivity of frozen and unfrozen soil, n=dimensionless parameter which converts air temperature to surface temperature, CFI=cumulative freezing index, and L=volumetric latent heat of fusion.

The assumptions in ModBerg equation are the following:

1. Surface temperature will drop from annual mean air temperature to a value equal to averaged frost daily freezing index and will remain constant during the entire freezing season;
2. Heat transfer between soil layers is one-dimensional;
3. Prior to freezing, soil temperature is equal to its mean annual.

FROST Model

FROST (Finite Response of Soils at All Temperatures) is a finite-element model that predicts frost depth in soils. This model was developed by Dr. Wade Lein at the Cold Regions Research and Engineering Laboratory (CRREL) to be incorporated into the PCASE (Pavement-Transportation Computer Assisted Structural Engineering) software as the primary component for frost depth prediction.

FROST is based on the principal of pure energy balance as shown in Equation 2-1 (ERDC/CRREL TR-19-24):

$$\int_V \rho U dV = \int_S \dot{q}\, dS + \int_V , \qquad (2\text{-}1)$$

Where: V = the volume, S = the surface, $\dot{U}$ = the time rate of internal energy, q = the heat flux per unit area, and r = the external heat source per unit volume.

A layered system in the FROST model is then defined, using Equation 2-1, and the thermal conductivity and specific heat of each layer (material). Thermal conductivity and specific heat are defined according to Equations 2-2 and 2-3, respectively:

$$K = k_s^{\theta_s} * k_w^{\theta_w} * k_i^{\theta_i}, \quad (2\text{-}2)$$

$$C = \rho_s c_s \theta_s + \rho_w c_w \theta_w + \rho_i c_i \theta_i, \quad (2\text{-}3)$$

Where: K = the effective thermal conductivity of the soil system, k = the thermal conductivity of the soil component, θ = the component's volume fraction, s = soil, w = water, i = ice, C = volumetric heat capacity, ρ = a component's density, and c = a component's specific heat capacity.

Based on the equations above, it can be established that the FROST model requires several inputs including: soil volume fraction, thermal conductivity, specific heat, water volume fraction (also known as moisture content), and porosity. All of these properties are dependent soil type and location. It is also noted that, as discussed in ERDC/CRREL TR-19-24, two main assumptions were made for the current version of FROST model:

1. Due to ABAQUS (software package used to develop the model) limits on keeping moisture content as constant within a layer, no modelling of moisture flow through soils was employed; and
2. Porosity was kept at constant with no change in porosity due to ice formation within a layer.

Frost-Depth Predictions in Real-Life Conditions

Field testing of frost depth penetration was conducted by various researchers. For instance, Nordal and Hansen (1982) performed evaluated frost penetration depth on a roadway segment section in northeast of Oslo, Norway. The researchers also studied the impact of spring thaw on the pavement's load-bearing capacity. Nordal and Hansen (1982) observed that the bearing capacity of the pavement decreased with every thaw cycle, varied with the actual frost conditions, and was material-dependent. After a cold winter (1962-1963), Nordal and Hansen (1982) reported that the increase of thaw depth increased deformations in the pavement structure. The maximum deflection was observed right before the end of the spring thaw or a couple of days later. Nordal and Hansen (1982) also observed that sections with a clay subgrade, suffered the highest deformations and the results of the bearing capacity tests performed on these sections showed consistency between the degree of frost heave formation and maximum deflection. For sections with silty subgrade, the deformations were relatively small and not influenced by frost heave formation.

Chamberlain (1981), tested four roadway sections between Springfield, IL, and Duluth, MN (Chamberlain, 1981). The sections had silty and sandy clay subgrades. Chamberlain (1981) focused on seasonal variation in deflection and considered the number of freeze-thaw cycles, type of subgrade and frost depth in the study. It was reported that no relationship between the freezing index and the maximum deflection during spring thaw exists; thus, freezing index is not a good predictor of load carrying capacity (Chamberlain, 1981). Chamberlain (1981) also observed that a soil's frost

susceptibility classification is the most significant variable affecting pavement deformation.

McHattie (1980) evaluated 120 flexible pavements in Alaska. The goal of this study was to assess the deformations in the pavement structures and how such deformations influence performance. Each section was classified based on cracking, rut depth, and maximum deformation. Materials from each section were tested for: particle size distribution, moisture content and the rate of frost heave formation. McHattie (1980) concluded that the percentage of particles smaller than 0.075mm in the base and subbase layers directly affected cracking of asphalt layer and load-carrying capacity of pavement structures during spring thaw. The maximum deflection during spring thaw was found to be directly proportional to the degree of asphalt layer cracking. Other results showed no correlation between freezing index and bearing capacity (McHattie, 1980).

A comprehensive field study with the goal of evaluating the impacts of frost action was conducted by the Joint Highway Research Project on 30 New Jersey soils and subbase materials (Turner and Jumikis, 1956). Vertical displacement and loss of bearing capacity during the cold season, and the recovery of the bearing capacity during spring and summer were measured for these soils (Turner and Jumikis, 1956). From all the soils used, 22 were representative of 75 percent of New Jersey soils, while 8 were typical subbase soils used in highway construction. Pavement slabs were placed on top of the soils to simulate field conditions. Plunger weights acting as static load were used as a measure of bearing capacity. Along with the tests performed for analyzing the soils' bearing capacity, concrete slabs were poured on top of each material (soil) for studying the frost-heave, measured by the daily movement of these slabs during winter.

The instrumentation plan employed by Tuner and Jumikis (1956) is presented in Figure 4. Freezing took place due to the existence of the natural groundwater table and no controlled saturation was considered. The results of this study revealed that the bearing capacity of soils decreased as result of freeze-thaw conditions and precipitations. Moreover, it was determined that bearing capacity of soils is moisture dependent and it is higher in soils with lower moisture contents (Turner and Jumikis, 1956).

Figure 4

Instrumentation Used for Evaluating the Bearing Capacity of New Jersey Soils at Rutgers University (K.A. Turner & A.R. Jumikis, 1956)

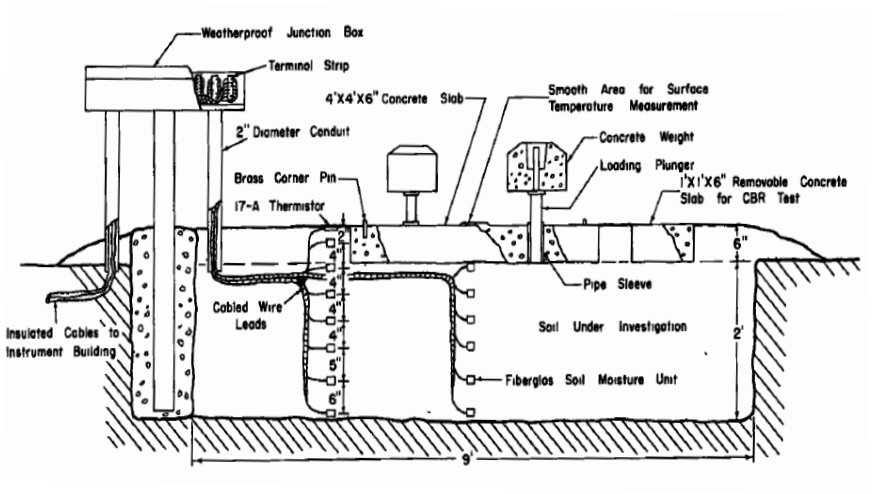

Zhang and Macdonald (2003) used a Danish Road-Testing Machine (RTM) to measure a pavement's mechanical responses (stresses and strains) under thaw periods of three freeze-thaw cycles inside an environmentally controlled building (Figure 5). The Test was repeated three times for different pavement structures and using different wheel loads. For the first Test (RTM1), dual wheel loads ranging between 20 kN and 40 kN were applied for 50,000 repetitions for each loading magnitude. The second test (RTM2),

conducted a year later, involved using dual tire half-axle loads of 40kN, 50 kN and 60 kN. The flexible pavement structure consisted of bituminous top layer over crushed natural gravel Base, on top of a low-plasticity clayey-silty-sandy-gravel subgrade. The last Test (RTM3) was based on RTM2, except a thickened top asphalt layer was used and a constant wheel load of 60 kN was applied (Zhang and Macdonald, 2003).

The instrumentation used in Zhang and Macdonald (2003) consisted of horizontal asphalt strain gauges (ASGs), soil pressure cells (SPCs), and soil deformation transducers (SDTs). The pavement temperature was also monitored using thermocouple probes (TMPs) to evaluate the freezing condition of the pavement.

Both (RTM2 and RTM3) studies showed that in pavements with unbound granular subgrades, the rate of pavement deterioration caused by thaw weakening, was orders of magnitude higher in subfreezing regions comparing to regions with above freezing climates.

Figure 5

The Danish Road-Testing Machine (Zhang & McDonald, 2003)

Summary of Literature Review

The literature review presented previously was conducted by researching different aspects related to freeze-thaw in flexible pavements. Among these are pavement's exposure to frost action, frost-heave formation and seasonal variations of impacts on resilient modulus and pavements' load bearing capacity. The following points provide a summary of the main findings from the literature review conducted as part of this study:

- Cold weather penetrates a pavement structure causing the water between soil particles to freeze. The frozen water, in turn, increases the load-bearing capacity of the frozen unbound layers. However, water expands when frozen, leading to the formation of frost heave and ultimately cracks in the upper pavement layers;
- Three conditions are required, simultaneously, for frost heave to form. These include: 1) existence of cold weather penetrating the pavement structure, 2) presence of water in or close to unbound pavement layers, and 2) presence of frost susceptible soils with capillary support ability to hold moisture (poor drainage);
- During spring thaw, a large amount of water is trapped between soil particles, saturating the unbound layers in pavement structures. The presence of water in unbound layers (especially the subgrade) reduces the shear strength of these layers and their resilient modulus. This in turn leads to reduced load-bearing capacity in pavement structure. Such pavements also experience excessive settlement (or deformations) when the water is drained out of unbound layers;
- A frost-susceptible soils are defined as "soils in which significant detrimental ice segregation will occur when the requisite moisture and freezing conditions are present" (USACE, 1984). Particle sizes finer than 0.02mm and Atterberg limits

are typically used to classify a soil type as potentially frost-susceptible or non-frost-susceptible according the U.S. Army Corps of Engineers guidelines (USACE, 1984); and,

- Several methods for estimating frost depth penetration in layered systems exist. These include the ModBerg model and the FROST model developed at CRREL.

Chapter 3

Materials and Laboratory Experimental Program

Chapter 3 provides a discussion of the materials evaluated in this study and the experimental program implemented. A total of 16 different types of soils were collected from various supplies in New Jersey (NJ). The goal of such evaluation was to select two materials that are frost-susceptible and for use in construction of full-scale pavement sections. Additional details are provided in the following subsections.

Materials Evaluated

To identify two frost-susceptible soils from materials in NJ, a total of 16 paving materials suppliers were contacted and samples were collected from them. Table 3 presents where these materials were obtained from in NJ. As can be seen from Table 3, materials from Southern and Northern NJ were obtained. All these materials were either soils or aggregates.

Once samples from all materials were collected, a sieve analysis of each of these materials was conducted to determine the ones that have the highest potential of being frost-susceptible. Figure 6 presents the sieve analysis results for all 16 materials. The potential for frost susceptibility of the materials tested was based on the particle size distribution criteria discussed in Chapter 2. That is, the higher the proportion of particles finer than 0.02 mm, the more frost-susceptible is the material. Since only a sieve analysis was conducted at this stage of the study for all 16 materials, the rational way was to select the three materials with the highest percentage of particles finer than 0.075 mm (or sieve

No. 200). As shown in Figure 6, Soils #2, #13, and #16 had the highest percentage of particles passing sieve No. 200; thus, they were selected for further analysis.

The selected soils were then tested for specific gravity and hydrometer analysis to verify their level of frost susceptibility based on the particle size criteria (Chapter 2). Figure 7 presents the results of these tests. As can be seen from Figure 7b, both Soils #2 and #13 had the highest percentages of particles finer than 0.02 mm (18.16% and 5.88%, respectively; thus, they are the most frost-susceptible. These two soils were selected for further testing as described in the experimental plan in the following section. It is noted that the specific gravity test was conducted to facilitate calculating the particle size distributions from the hydrometer analysis.

Table 3

Locations in New Jersey from which Soils were Obtained

Soil No.	Description from Supplier	NJ Location
Soil #1	Sand	South Jersey
Soil #2	Sandy Clay Borrow	South Jersey
Soil #3	Martin	South Jersey
Soil #4	Naceville	South Jersey
Soil #5	I-15	South Jersey
Soil #6	DGA Commercial	North Jersey
Soil #7	Type G Fill	South Jersey
Soil #8	RCA	North Jersey
Soil #9	Pond Fill	North Jersey
Soil #10	Fill	North Jersey
Soil #11	Paver Sand	North Jersey
Soil #12	Dead Sand	North Jersey
Soil #13	Pond Fill 2	North Jersey
Soil #14	Select Fill	Delaware
Soil #15	Screenings	North Jersey
Soil #16	Pipe Sand	North Jersey

Figure 6

Sieve Analysis Results of All Materials (Soils and Aggregates) Samples Collected

(a) Soils 1 through 4

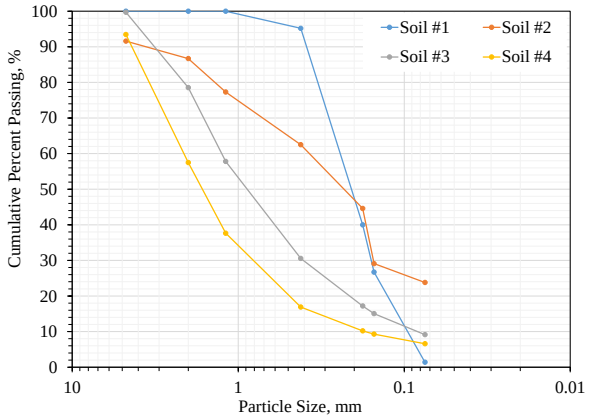

(b) Soils 5 through 8

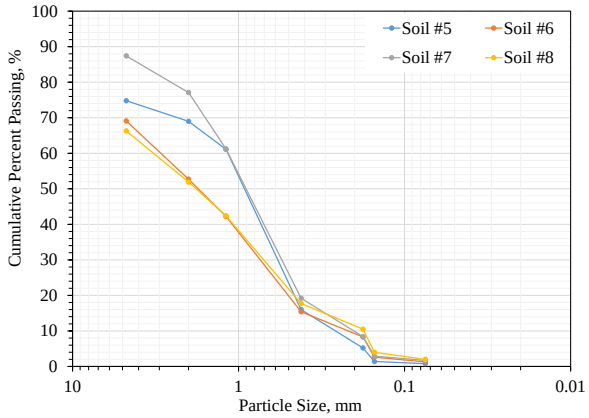

(c) Soils 9 through 12

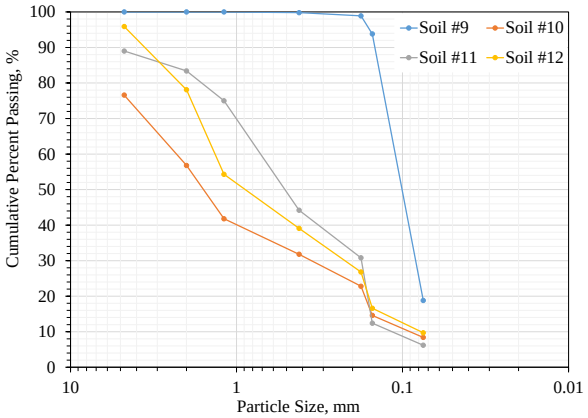

(d) Soils 13 through 16

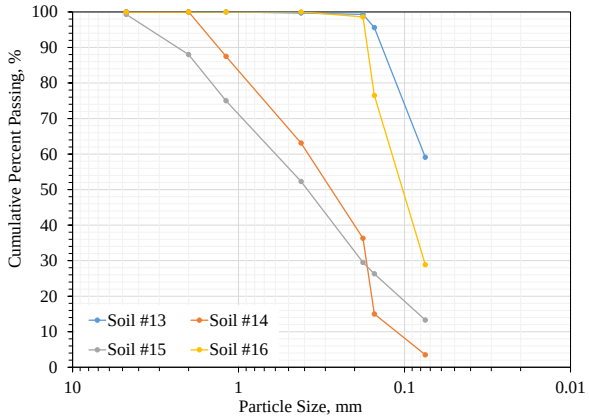

Experimental Program

Upon identifying frost-susceptible soils, additional testing was conducted to further characterize these soils. The measured properties for the current soils were necessary for specifying materials properties for full-scale construction. The properties are also used as inputs into the FROST model discussed in Chapter 2. Table 4 presents the experimental program for this study. As shown in this table, the tests included: soil classification and Atterberg limits, compaction tests (Proctor), and strength and properties tests (California Bearing Ratio, CBR, and resilient modulus). A description of each of these tests is provided in the following subsections.

Table 4

Experimental Testing Program of Selected Soils

Test	Soil #2	Soil #13
Specific Gravity (ASTM D854-14)	✓	✓
Particle Size Analysis (ASTM D1140. D6913, & D7928)	✓	✓
Atterberg Limits (ASTM D4318)	✓	✓
Standard Proctor (ASTM D698)	✓	✓
California Bearing Ratio (CBR, ASTM D1883)	✓	✓
Resilient Modulus (AASHT T307)	✓	✓

Figure 7

Specific Gravity and Hydrometer Analysis Results for Soils #2, #13 and #16

(a) Specific Gravity

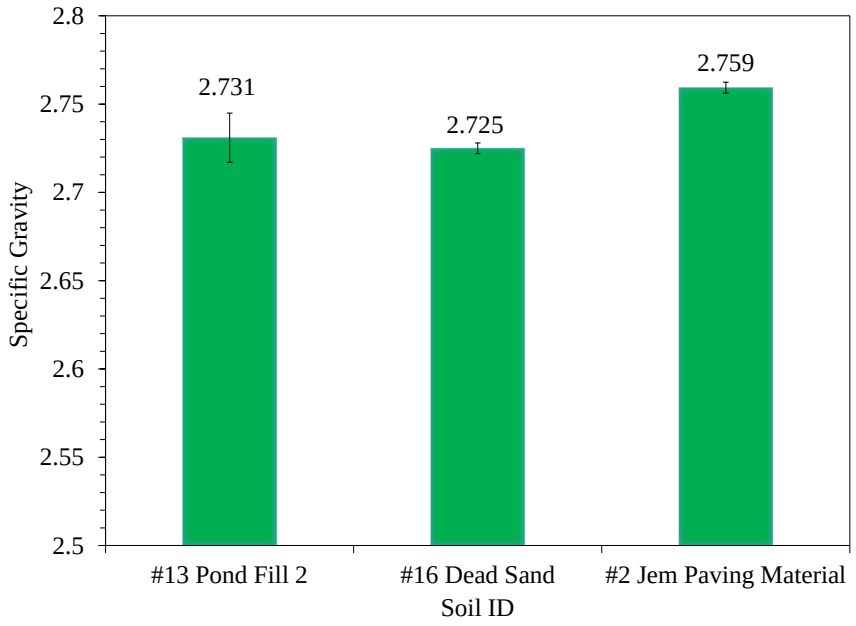

(b) Gradation Containing Hydrometer Analysis Results

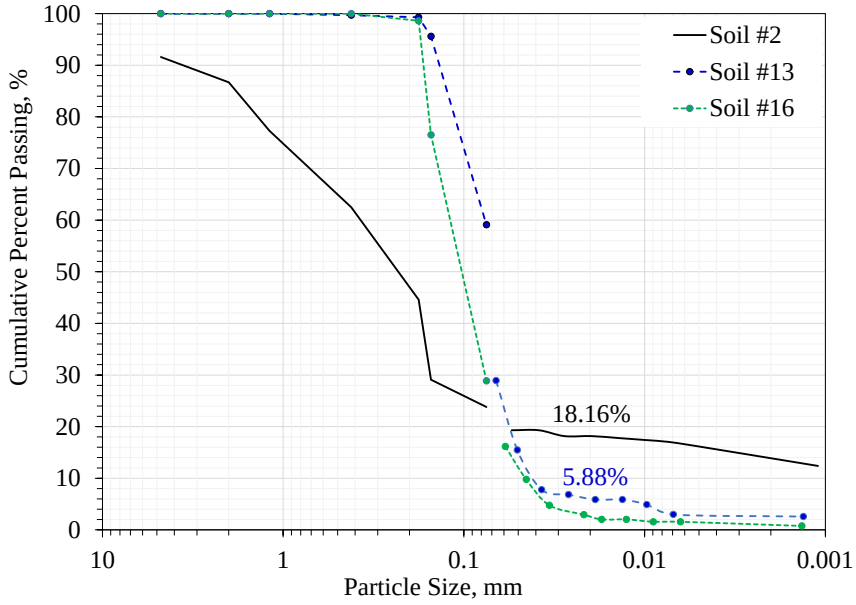

Specific Gravity

The specific gravity of the selected soils was determined according to ASTM D 854-14 standards using a pycnometer. In this test, soil samples were sieved through a #10 sieve prior to testing. Samples were soaked for approximately ten minutes inside a pycnometer and then exposed to partial vacuum for another ten minutes in order to remove any entrapped air. Once vacuum was applied for 10 minutes, the pycnometer was filled with water to a marked level. The specific gravity was determined as the ratio of the mass of unit volume of soil at the test temperature to the mass of the same volume of distilled water at the same temperature. Three replicates per soil type were tested tests for specific gravity. The average of the three replicates is reported as the specific gravity of a soil type.

Particle-Size Analysis

The particle-size analysis involved conducting dry sieve analysis (ASTM D6913), washed sieve analysis (ASTM D1140), and hydrometer analysis (ASTM D7928). As discussed previously, these tests were conducted to determine if the soils are frost-susceptible based on the particle size criterion (i.e., percentages of particles finer than 0.075 mm).

Washed sieve analysis was conducted according to ASTM D 1140-17 to determine the percent of particles finer than 0.075 mm. After the washing cycle, the material was dried in the oven at 110^{o}C for 16 hours and then tested in conformity with ASTM D 6913, using a mechanical sieve shaker for a shaking period of 15 minutes. Materials passing sieve No. 200 were kept for further testing in the hydrometer analysis.

The hydrometer test was performed following ASTM D 7928. The goal was to determine the percent of particles finer than 0.02 mm by weight. The sieve analyses tests (ASTM D1140 and D6913) were performed to determine the distribution of coarse (gravel and sand) particles, while the hydrometer was used to determine the distribution of finer particles (clays and silts).

Atterberg Limits

Atterberg limits tests were performed following ASTM D 4318. The soils were tested to determine the Liquid Limit (LL), Plastic Limit (PL), based on the moisture content of the soil, and then the Plasticity Index (PI) was determined using the relationship PI=LL-PL. Since the soils were crumbling easily, the rolling method could not been performed. The PL was determined using the Falling Cone Penetrometer (IS 2720).

The LL is the moisture content that defines where the soil changes from a semi-solid to a plastic (flexible) state. The LLs for the soils were determined using a Casagrande machine. The soil samples were sieved through a 425μm sieve, mixed with water and then placed into the cup of the apparatus. A grooving tool was used to cut a straight groove down the center of the cup. The machine was used to count the number of drops it took for the both halves of the soil samples to come into contact. Once in contact, the machine would be stopped and a sample taken out of the cup and placed in the oven for moisture content determination.

The above procedure was repeated for different moisture contents in such a manner so for the same soil sample would be obtained a different number of drops; one

of the trials for a closure requiring 15 to 20 drops, one for a closure between 20 and 25, one for a closure between 25 and 30, and one for a closure between 30 and 35. The results were plotted for moisture content as a function of number of drops.

The Plastic Limit (PL) is the moisture content that defines where the soil changes from a plastic state to a viscous state. The PL was determined using the IS 2720 standard. The apparatus used was a cone penetrometer with a carriage mass of 240g. The soil sample was passed through a 425μm sieve and mixed with water to obtain a uniform paste. The wet soil was placed into a cylindrical cup, leveled up to the top of the cup and placed on the base of the cone penetrometer apparatus. The penetrometer was adjusted so the cone point just touches the surface of the soil paste. Then the cone was released allowing it to penetrate into the soil paste under its own weight for 5 seconds. The penetration was registered to the nearest millimeter. The test was repeated for different moisture contents in order to obtain values of penetration between 14-28 mm. A sample of the tested soils was dried in the oven for moisture content determination.

The Plasticity Index (PI) is the difference between the water contents of soil in viscous and plastic state, and is an important factor in classifying fine-grained soils. The PI was determined by subtracting the PL value from the LL value for each test. The data collected from these tests was used to classify the soils according to the Unified Soil Classification System (USCS), performed following the ASTM D 2487-17 standard.

Standard Proctor Compaction Test

The standard Proctor compaction test was performed according to ASTM D 698 standards. The goal of this test was to determine the Optimum Moisture Contents (OMC)

and the corresponding Maximum Dry Densities (MDD) for the selected soils (i.e., establish moisture-density relationships). The standard proctor method was performed, using a 5.5 lbs. hammer falling from a height of one foot into a mold filled with moist soil. The mold was filled in three lifts, each subjected to 25 hammer drops. Depending on the materials' gradations, either a 4-inch or a 6-inch mold was used to perform the compaction test. Once compaction of three lifts was completed, the mold was weighed its wet density is calculated (soil weight divided by mold volume). A sample was then collected from the middle of the mold to measure the actual moisture content of the soils in the mold. These moisture samples were dried for 16 hours. The test was conducted at different moisture contents.

The relationship between the moisture content of the soil and its dry density, allows identifying the necessary water content to be added to a soil mass for a desired compaction rate. The data obtained from compaction tests was used in comparing the density obtained in the field, after constructing the full-scale sections (Chapter 5), with the density obtained in the lab on samples of the same soil.

Strength Tests

California Bearing Ratio (CBR). The CBR test was used to determine the strength of the selected soils. The test was performed according to D1883-16 standard, which applies for laboratory compacted soil samples. In this test, the soils were sieved through a 3/4-inch sieve and the particles retained on this sieve were removed prior to testing. A 6-inch mold and a standard hammer were used to prepare the samples. A Materials Testing System (MTS) loading frame and a penetration cylinder were used for testing. The compacted sample was subjected to penetration rate of 0.05 in./min. The CBR values corresponding to each soil sample were determined as the penetrations at either 0.1 in. or 0.2 in., by dividing the corresponding recorded load by 1000psi or 1500psi respectively. Multiple CBR tests (three replicates) were performed for the selected soils.

Resilient Modulus. The Resilient Modulus test was performed in conformity with AASHTO T307-99 standard. The test was performed using different loading sequences and confining pressure values, based on standards. The goal of this test was to determine the resilient modulus values of soils, simulating real conditions of a pavement structure exposed to wheel loading. The Resilient Modulus testing was performed using a Triaxial Pressure Chamber and an MTS machine programmed to perform a pulse-type dynamic loading.

The soil sample was tested at the optimum moisture content. A 71-mm mold was used for the test. The soil was compacted in six lifts in a split mold with an air tight membrane, placed on the base of the triaxial cell. A vibratory impact hammer with a 70-

mm cylindrical head attachment was used for the compaction process. Once compacted, the sample was placed inside the triaxial chamber, with two LVDTs connected to the top. Then the chamber was connected to the pressure supply line and a confining pressure was applied. The sample was conditioned for 500 cycles under a confining pressure of 103.4 kPa.

Two test procedures were performed; one for the subgrade and one for the base. The procedure for base and subgrade differed by confining pressure and maximum axial stress applied.

Chapter 4

Laboratory Results Discussion

In this chapter, a discussion of the laboratory characterization of the two frost-susceptible soils selected in Chapter 3 is presented. Specifically, this chapter includes the Atterberg limits, soils classification, moisture-density relationships (Proctor), California bearing ratio (CBR), and resilient modulus (M_r) results as presented in the following sections.

Atterberg Limits

The liquid limits for both materials (Soil #2 and #13) are presented in Figure 8. As illustrated in this figure, the liquid limit for Soil #2 is 22.31 % while for Soil #13 it is 28.89%. Both of the soils are; therefore, capable of absorbing a large portion of water before reaching a liquid flow state.

Figure 8

Liquid Limits (LL) for Soils #2 and #13

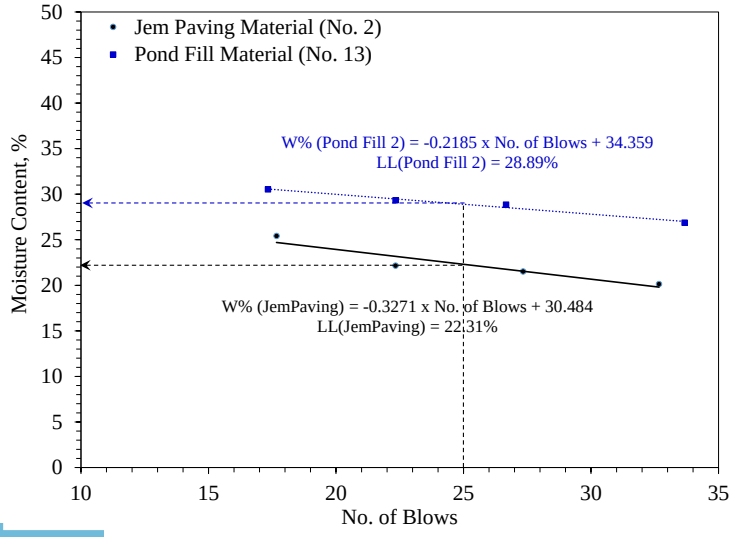

Figure 9 presents the plastic limit and plasticity index (liquid limit – plastic limit) values for both Soils #2 and #13. As can be seen from this figure, Soil#2 had a plastic limit of 17.74% while Soil #13 had a plastic limit of 27.44%. The plasticity index values for Soils #2 and #13 were 4.57% and 1.45%, respectively. Since both soils had plasticity index values less than 7, both materials are considered to be slightly plastic (Sowers, 1979).

Figure 9

Plastic Limit (PL) and Plasticity Index (PI) for Soils #2 and #13

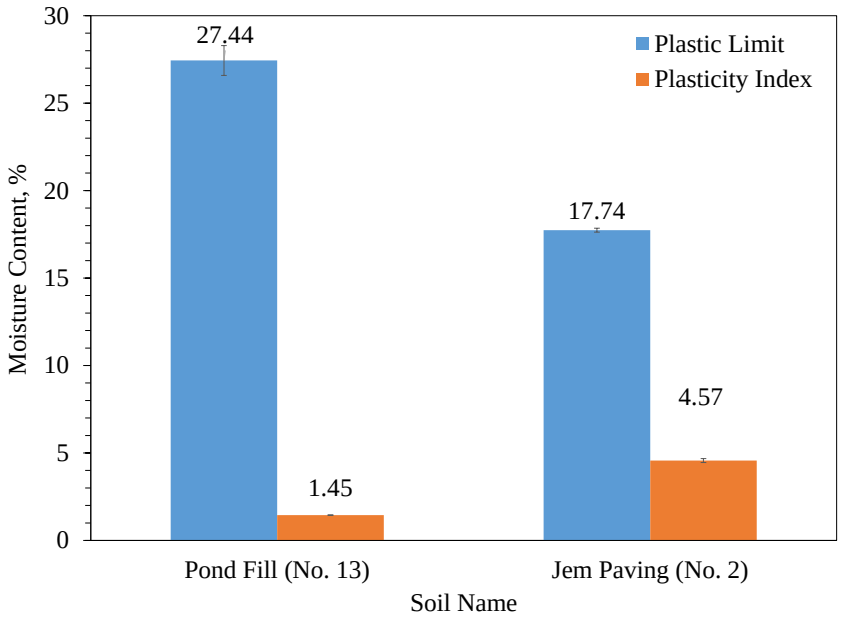

Classification of Soils #2 and #13

The Unified Soil Classification System (USCS) was used to classify Soils #2 and #13. For that reason, the Atterberg limits, Plasticity Index values, and soil sieve analysis results (i.e., percent of particles finer than Sieve No. 200) were used to classify the soils.

The classification of Soil#2 and Soil#13 is shown in Table 5. As can be seen from this table, Soil #2 is classified as low plastic Clayey Sand (SC) and Soil #13 as low plastic inorganic silt (ML).

Using the hydrometer analysis results (% finer than 0.02 mm in Chapter 3), both soils #2 and #13 can also be categorized as frost susceptible. Based on the USACE definition of frost susceptible soils, both materials fall under the F3 and F4 groups, respectively. Soil#2, classified as Clayey Sand (SC), had 35% (over 15%) of particles smaller than 0.02mm by weight and was assigned to subgroup F3(b), while Soil#13 , Low Plastic Silt (ML), with 55% of particles smaller than 0.02mm by weight, is included in subgroup F4(a).

Table 5

Classification of Soils #2 and #13 Using the Unified Soils Classification System (USCS)

Soil	% Finer #200	Liquid Limit (%)	Plastic Limit (%)	Classification Factors			Soil Type
#2	46	22.31	17.74	>50% Retained on #200 sieve	LL <50%	PI<7	LOW PLASTIC CLAYEY SAND (SC)
#13	92	28.89	27.44	>50% Passing #200 sieve	LL <50%	PI<7	LOW PLASTIC INORGANIC SILT (ML)

Moisture-Density Relationships

The moisture-density relationships as obtained from the standard Proctor test for both Soils (#2 and #13) are presented in Figure 10. From this figure it can be seen that the inorganic silt (ML, Soil #13) soil had a higher Optimum Moisture Content (OMC) (17.1 %) than Soil #2. Soil #13 also had a lower Maximum Dry Density (MDD) (1.73 g/cm3) than that measured for Soil #2. As seen from the figure, the MDD density value for the Clayey Sand (SC), increases (2.08 g/cm3) as the OMC values decrease (11.61 %). For soils having a higher OMC, the density has a smaller value as water tends to replace soil particles (less weight).

Figure 10

Moisture-Density Relationships for Soils #2 and #13

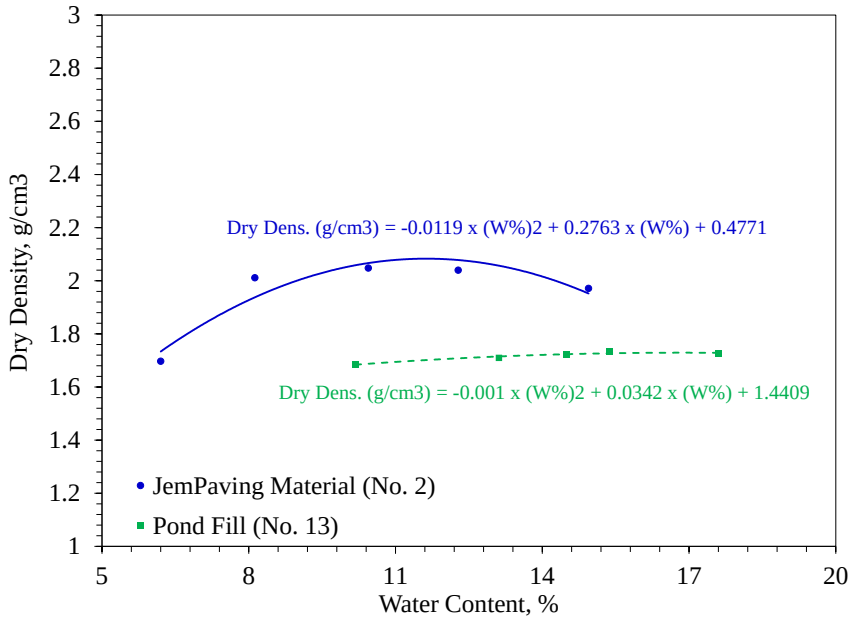

California Bearing Ratio (CBR)

CBR results for both soils are presented in Figure 11. Both soils were compacted at Optimum Moisture Content (OMC). Soil #2 (SC) had an average CBR value of 7.1% recorded at 2.5 mm penetration. Soil #13 (ML) had higher OMC value of 7.8% at a 5 mm penetration. Based on typical CBR values (Yoder and Witczak, 1975), CBR for SC-type soils ranges between 10-20% with these soils recommended for use as pavement foundation, when not subjected to frost action. On the other side, ML-type soils provide have a fair to poor (between 5 and 15%) CBR values for use as base or sub-base layers. Therefore, both Soil #2 (SC) and Soil #13 (ML) are considered very weak soils and unsuitable as base and sub-base layers for pavements (that is, their measured CBR values are less than 10%).

Figure 11

California Bearing Ratio Values for Soils #2 and #13

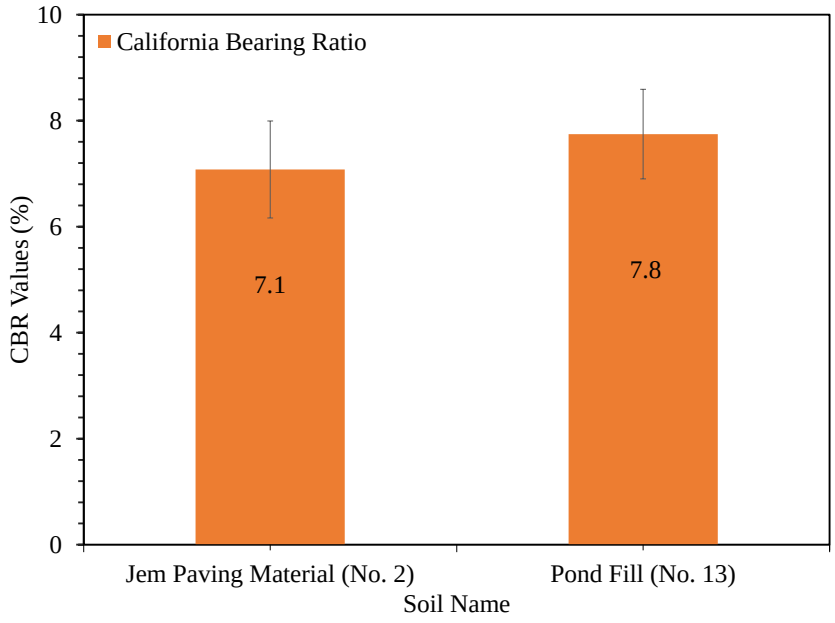

Resilient Modulus

Resilient Modulus (M_r) testing was performed on samples of soils compacted at OMC from Proctor test. Figure 12 shows the average results for Soil #2 (SC) tested for all fifteen loading sequences. It can be seen that the M_r values for Soil #2 (SC) had similar trends in all loading sequences (i.e., decreasing then increasing in M_r values) and had similar M_r values (between 45 and 50 MPa) when tested at different confining pressures and axial stress levels. In the guidelines for use of HMA overlays to rehabilitate PCC Pavements (NAPA, 1994), SC-type soils have typical M_r values between 48-103 MPa. This again suggests that while Soil #2 is classified as Clayey Sand, this material is weaker than typical.

When conducting the resilient modulus test on Soil #13 (ML), difficulties in operating a meaningful test were encountered. What occurred is that samples prepared from Soil #13 (ML) continuously failed during the conditioning phase of the test. The conditioning phase involves exposing the sample to 500-1000 cycles under a confining pressure and maximum axial stress specified by the standard (AASHTO T307). The conditioning is performed to eliminate the effects of interval between compaction and loading, and minimize the effects of initially imperfect contact between the sample cap and base plate and the test specimen. Figure 13a shows a picture of Soil #13 sample failure due to exceeding the allowable vertical strain. AASHTO T307 standard states that during the conditioning phase, a soil sample should not exceed a permanent vertical strain of 5% for the test to continue. Figure 13b shows a total failure of a Soil #13 (ML) sample due to high shear stresses caused by weak interlock between the soil particles. More than 15 attempts were made to test Soil #13 with all of them failing at the conditioning phase.

Figure 12

Average Measured Resilient Modulus Values for Soil #2

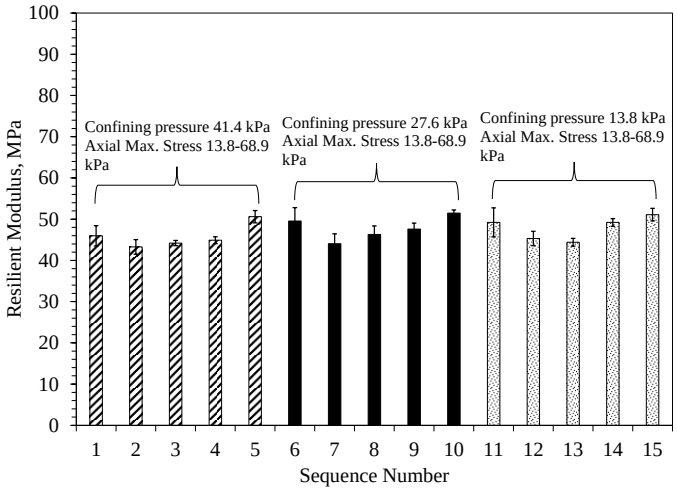

Figure 13

Pictures of Pond Fill (ML) Soil Samples in the Conditioning Phase of Resilient Modulus Testing

(a) High vertical strain

(b) Shear failure

Since Resilient Modulus Testing for Soil #13 (ML) could not be performed passing the conditioning phase, the use of an empirical relationship between CBR and Resilient Modulus was considered to estimate the M_r value for Soil #13 (ML). Based on Transportation and Road Research Laboratory (TRRL) Report LR. pp. 62, 1132 (Powell and Potter, 1984) the following relationship be-tween CBR and M_r was used (Equation 4-1):

$$M_r(MPa) = 17.6 \cdot CBR^{0.64} \quad (4\text{-}1)$$

The averaged estimated M_r value using Equation 4-1 and the laboratory CBR test results value for Soil #13 (ML) equals to 65.24 MPa.

Using the same relationship, the M_r value for Soil#2 (SC) was calculated at 61.58 MPa. This value exceeds the Resilient Modulus value obtained from lab testing, which indicates that the empirical relationship used above, overestimates the resilient modulus. It is also noted that this relationship may also not be applicable for clayey sand soils. Nonetheless, the guidelines for use of HMA overlays to rehabilitate PCC pavements (NAPA, 1994) suggest that both, SC and ML-type soils have typical M_r values between 48-103MPa. The measured (for Soil #2) and estimated values fall in this typical range.

Summary of Findings from Laboratory Testing

Laboratory testing was conducted to classify Soils #2 and #13, measure their properties (Atterberg Limits, CBR, and M_r) and assess their frost-susceptibility potential. Analyzing the test results and relating them to the literature findings, the following conclusions were highlighted:

- Both soils (#2 and #13) contained high amounts of fine particles. Soil #13 had a considerably higher amount of fine particles (Sieve No. 200) than Soil #2. Based on Frost-Susceptibility Classification (USACE, 1984), it was found that Soil #2 can be classified as F3(b) frost susceptible soils, while Soil #13 is classified as F4(a) frost-susceptible soils. Soils from groups F4 are considered highly frost-susceptible.
- Soils #2 and #13 had a low Plasticity Index values (PI < 7). This indicates that both soils have low plasticity.
- Soil #2 has a higher MDD compared to Soil #13. This suggests that Soil #2 is more compactable than Soil #13 (can reach higher densities in the field). Soil #13 also had a higher OMC than Soil #2; suggesting that this material may have higher permeability.
- Both soils, Soil #2 (7.1%) and Soil #13 (7.8%) showed low CBR values. Based on Iowa Statewide Urban Design and Specifications (2013), a very good base layer will have a CBR value between 50-80%, while a very good subgrade layer a value between 20-30%. Considering the CBR values above, both soils are considered weak and unsuitable as base and subgrade layers.
- While Soil #2 (SC) showed a low Resilient Modulus value (50 MPa), M_r was not measured for Soil #13 (ML) due to failure of samples during testing. A M_r value was estimated for Soil #13 (65 MPa) using an empirical relationship with CBR results. Overall, the M_r values for both soils (estimated and measured) indicate that they are both weak.

Chapter 5

Construction of Full-Scale Pavement Section

Chapter 5 presents a discussion of the activities undertaken to construct three full-scale pavement test strips for collecting data and evaluating the FROST model discussed in Chapter 2. A discussion of the materials used, based on findings from Chapters 3 and 4, for constructing these three strips is also presented in this chapter. In addition, instrumentation of the strips using thermal conductivity probes is presented.

Selection of Test Strips Location (Shadow Analysis)

A shadow analysis was conducted to determine the best location for placing the test strips (all three in one section). The location was selected to be closer to the entry gate so it is more accessible for the equipment and materials deliveries. Also, the location was selected to be further away from the building, so it is more exposed to solar radiation. The shadow analysis involved the use of Google Sketchup software that simulated the sun movement for a period of 12 months. The software used real coordinates (N39°43’7.1976” and W75°8’38.2884) for the section’s location and real measurements of the building and runaway were inputted as well. As seen from Figure 14a, the cardinal points were determined and the movement of the sun analyzed. Based on the sun’s movement, shadow movement was determined. Since the Heavy Vehicle Simulator (HVS) was constantly used, different positions of the HVS were analyzed and a shadow analysis was performed. It was determined that some HVS positioning will black-out the section (Figure 14b).

A more detailed one-day shadow analysis was also performed using a three-dimensional simulation. Figure 15 shows the area of the section captured at different moments of a day (January 15th of an arbitrary year). As seen from Figure 15, the area is completely exposed to the sun and no shadow is seen during the day with the sun movement.

Figure 14

Sun Movement and Shadow on Sections Selected Location

(a) Cardinal Points and Direction of Sun Movement

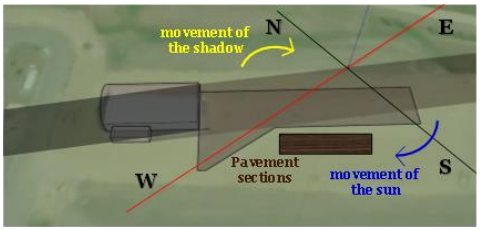

(b) Section covered by HVS shadow

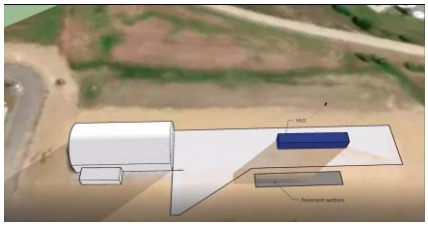

Figure 15

Shadow Analysis for January 15th at Different Times of the Day

The section's location (Figure 16) was chosen so the section gets as much sun as possible, since solar radiation is a factor that affects the thawing process.

Figure 16

Aerial Image of Test Strips Location

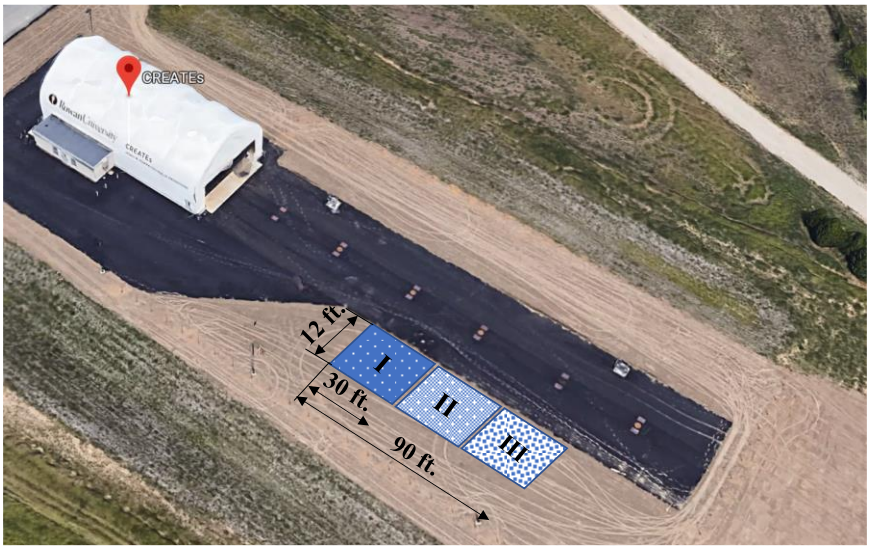

Pavement Sections and Materials

Figure 17 presents the pavement sections for all three test strips. As shown in this figure, all three test strips had a 3-inch thick hot mix asphalt (HMA) layer, a 6-inch thick base layer, a 27-inch thick subgrade layer, and a 7-inch thick aggregate filter layer to serve as a water reservoir. The whole pavement section was also insulated (using 4 ft. long by 8 ft. wide polystyrene boards) from the bottom and sides to ensure minimal impacts of surrounding ground temperatures on the test strips. To prevent water from seeping out of the section, an impermeable membrane (geotextile) was placed on top of the polystyrene boards (both on bottom and sides of section as shown in Figure 17). It is also noted that the whole section was 15 ft. wide and 90 ft. long with each strip being 30 ft. long. Once the strips were built and paved, 1-ft circular holes were drilled in the middle of each strip to facilitate installation of thermal conductivity sensors, and 4-inch holes were drilled at the edge of each strip to install saturation pipes.

The differences between the test strips were in the materials used for constructing the base and subgrade layers. As shown in Figure 17, Test Strip I was constructed using typical New Jersey Dense Graded Aggregates (DGA) and Soil #2 identified in Chapter 3. In Test Strip II, the base layer was constructed using a one to one blend of the DGA and Soil #13 while the subgrade contained Soil #2. In Test Strip III, a one to one blend of DGA and Soil #13 was used for the base layer and a one to one blend of Soils #2 and #13 for subgrade layer. Details of these materials are presented in the following subsection.

Pavement Sections and Materials

Hot Mix Asphalt (HMA). HMA mixture was purchased by the contractor and delivered to construction. This mixture was prepared using a PG 64-22 binder and aggregates graded to a Nominal Maximum Aggregate Size of 9.5 mm. Figure 18 shows that the optimum binder content for the HMA mix was 5.7%, meeting the requirements of 4% target air voids, 15% minimum voids in mineral aggregates (VMA), and 1-2% dust to binder ratio. The Bulk Specific Gravity (G_{mb}) of the HMA mix was 2.407, while the Maximum Specific Gravity (G_{mm}) was 2.508.

Figure 17

Structure of the Pavement Test Strips

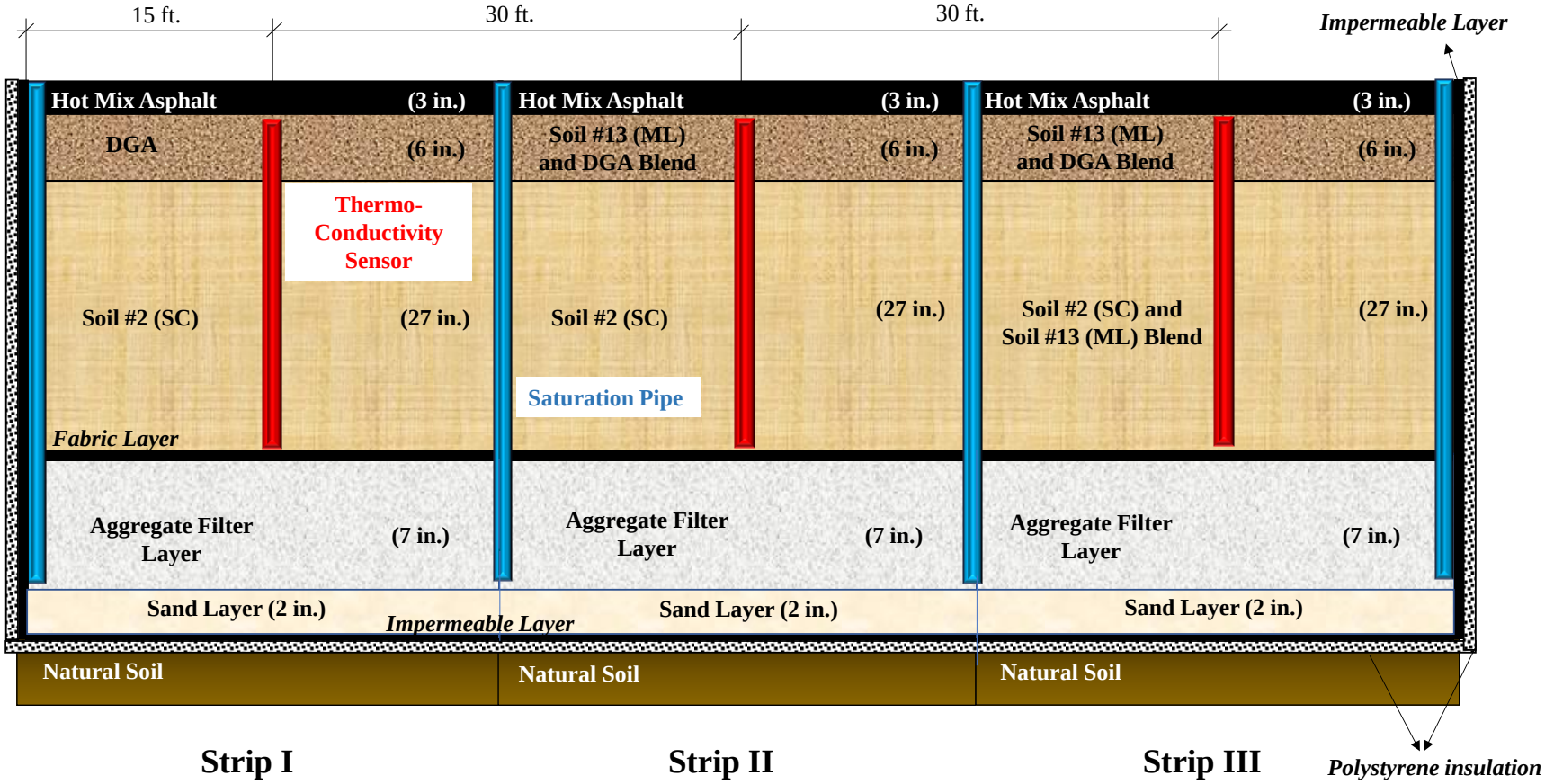

Figure 18

Gradation and Optimum Binder Content of Asphalt Mix

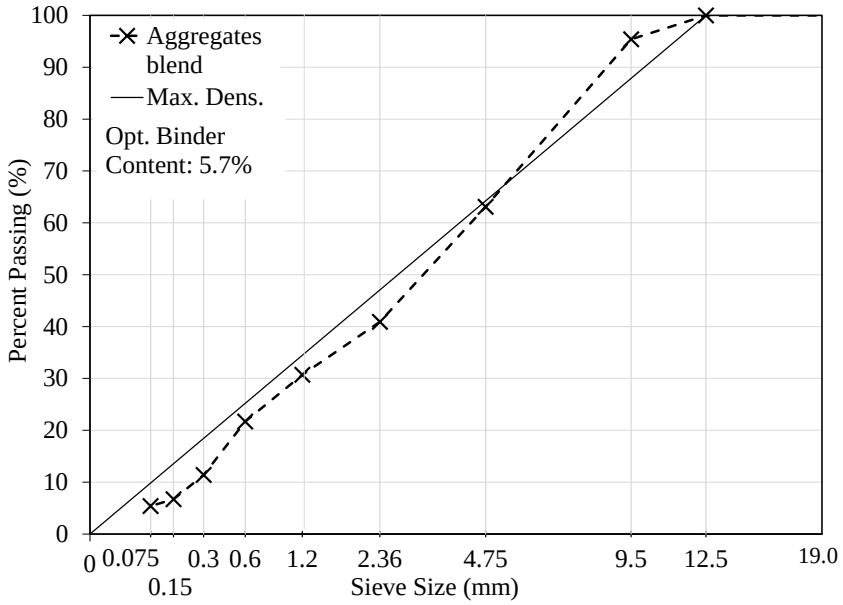

Base Layer (Dense Graded Aggregates and Blends). The base layer for Strip I was prepared using DGA (crushed stone). The base layer for Strip I was selected to be similar to a base layer of a regular road section. For Strip II and Strip III, a one to one blend of DGA and Soil #13(ML) was used. Since the goal of this study was building frost susceptible road sections, Strip II and III were designed to have a frost susceptible base layer, thus the DGA was blended with Soil #13 (ML) using a bucket loader. Both soils, DGA and Soil #13 (ML) were purchased form a local aggregate supplier.

Multiple tests were performed on the DGA, Soil #13 (ML) and the base materials blend (DGA and Soil #13) prior to construction start. Such testing was necessary to ensure these materials meet the desired properties (i.e., strong base layer and a hybrid base layer being somewhat more frost susceptible that typical base layers). The DGA and

blend of DGA and Soil #13 were tested for gradation, compaction, CBR and Resilient Modulus. The measured materials properties are summarized in Table 6. Figure 19 shows the gradation of these materials used as base layers.

Table 6

Properties of Dense Aggregate (DGA) and Blended Base Layer Aggregate

Property \ Soil	DGA	DGA and Soil #13 (ML) (1:1)
%Passing Sieve No. 200	4.3	47.8
OMC (%)	6.57	10.53
MDD (g/cm^3)	2.31	2.01
CBR (%)	54.6	35.96
M_r (MPa)	79.7-266.3	65.9-261.5

Figure 19

Gradation and DGA and One to One Blend of DGA and Soil #13

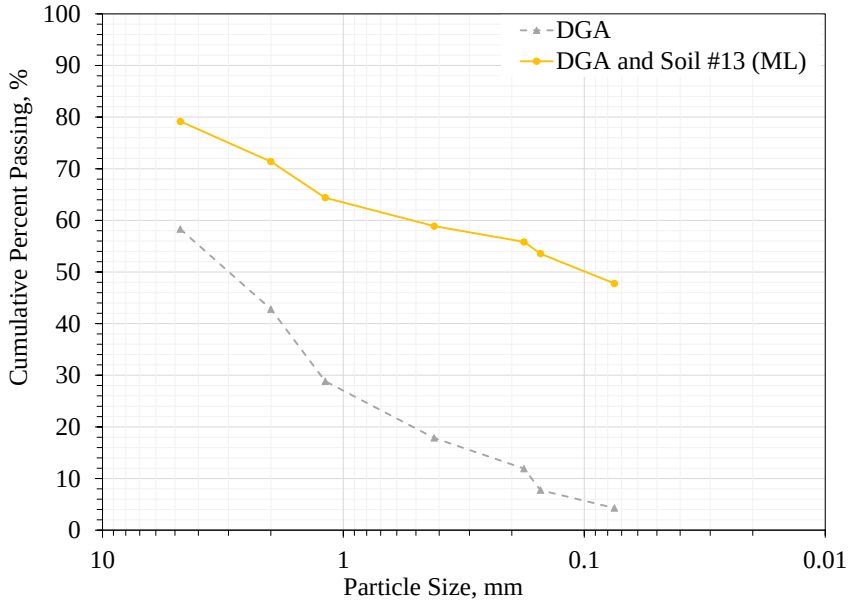

Subgrade Layer (Soil #2 and Blends). The subgrade layer for Strip I and Strip II consisted of Soil #2 (SC). This material was selected for two of the three test strips as it had a larger percent of particles smaller than 0.02 mm (see Chapter 3). This material also might have a higher surface area and a higher potential for holding water. Having such properties, Soil #2 is the most impacted by frost penetration from among all the 16 soils evaluated at the beginning of this study.

The subgrade layer in Strip III, a one to one blend of Soil #2 (SC) and Soil #13 (ML) was used. The soils were blended to have a different subgrade layer for analysis and comparison purposes (create a hybrid test strip with properties falling between Strips I and II). The blending process of these two soils was completed using a bucket loader (Figure 20).

Figure 20

Blending of Soils Using a Bucket Loader

Similar to base layer materials, both Soil #2 (SC) and the blend (Soil #2 and Soil #13) were tested for sieve analysis, Atterberg limits, compaction, CBR and Resilient

Modulus. The gradation for Soil #2 (SC) and the Blend (Soil #2 and Soil #13) are shown in Figure 21. The properties of soil #2 and the blend (Soil #2 and Soil #13, 1:1 ratio) are presented in Table 7. It is noted that differences in results between Soil #2 and Soil #13 can be observed when comparing Figure 21 with Figure 7b. At the beginning of the study, the materials suppliers were requested to sample and ship their materials to Rowan University. These initial samples provided by the suppliers provided an idea of how frost susceptible they might be. When looking at the results presented in Figure 21, it can be clearly seen that these materials are more frost-susceptible than initially tested.

Figure 21

Gradation of Soil #2 and Blend (Soils #2 and #13) Used as Subgrade Layers

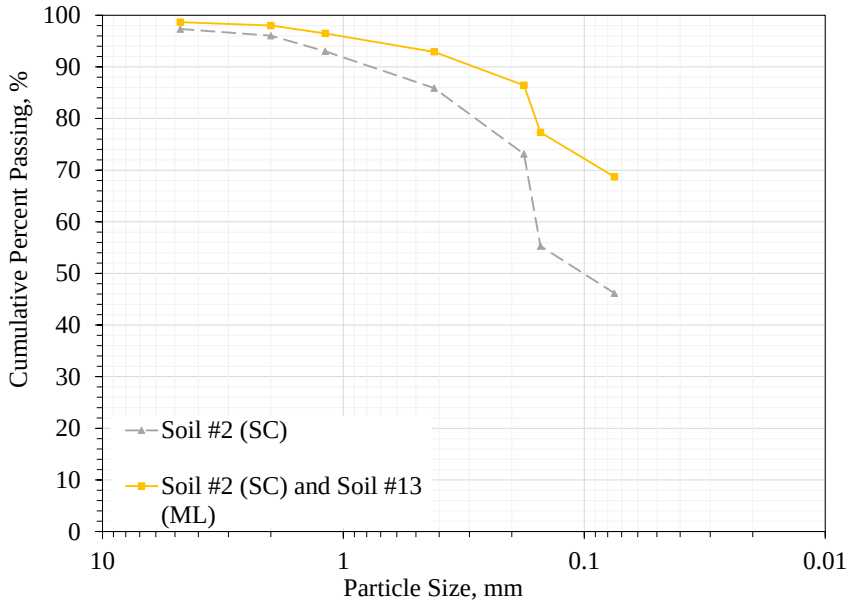

Filter Aggregates. The filter aggregate layer consisted of uniform 3/8-inch crushed bluestone. The crushed bluestone was purchased from local aggregate supplier and was used as a reservoir for water retention at the bottom of all three test strips.

Table 7

Classification of Soils #2 and #13 Using the Unified Soils Classification System (USCS)

Property \ Soil	Soil #2 (SC)	Soil #2 (SC) and Soil #13 (ML) (1:1)
%Passing Sieve No. 200	46.1	68.7
LL (%)	26.08	20.18
PI (%)	11.55	5.55
OMC (%)	15.43	13.65
MDD (g/cm^3)	1.8	1.85
CBR (%)	17.63	15.25
M_r (MPa)	45.9-58.4	62.8-75.4

Construction Activities

Surveying and Excavation

The first step of construction was to survey the selected location and identify current elevations in reference to a side point. For this purpose, the contractor, who was awarded this work, marked the location of the section (Figure 22) using a string and by measuring the required length (90 ft.) and width (15 ft.). The contractor then used a laser surveyor to determine the excavation depths at different points along the sections (Figure 22b). Since the ground was slightly inclined, the highest point along the perimeter was determined and selected as reference point for the excavation depth (Figure 22c).

Once rough excavation depths were reached, the contractor then used a crawler excavator (Figure 22a) to remove excess soil and create the excavation. The higher side

was excavated first while moving towards the lower side of the section. During excavation, multiple depth measurements were taken (Figure 23b and 23c). Once the pit hole reached the desired depth, the bottom and side walls were cleaned and leveled using manual labor, and at the end, the bottom was compacted using a drum compactor (Figure 23) and the depth was checked again by the contractor in multiple locations. As shown in Figure 23e, the final depth check was done by pulling a string diagonally from one corner of the section to another (projected HMA surface) and then using a measuring tape to measure depth from string down.

Figure 22

Pictures of Making and Surveying of Section

(a) Marking Perimeter

(b) Laser Surveyor

(c) Reference Point for Excavation

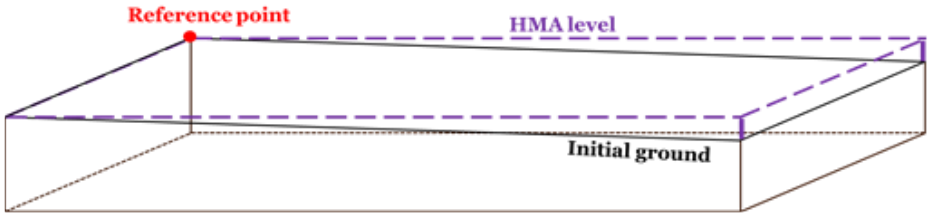

Figure 23

Pictures of Excavation Process and Depth Evaluation

(a) Crawler Excavator

(b) Depth Check Using Tape Measure

(c) Depth Check when Excavating

(d) Compaction Process

(e) String Reference Points.

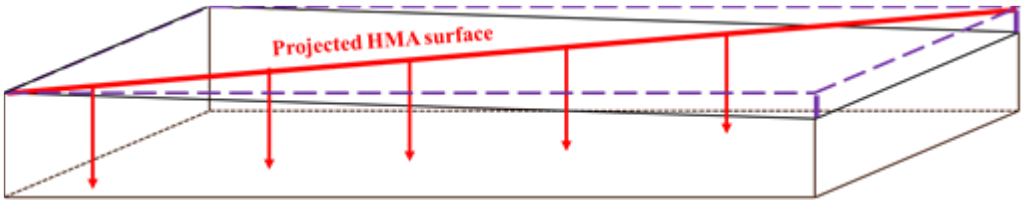

Once excavated, the hole was checked for quality control measurements (Depth, Width, Length, and Levelness). Table 8 presents the collected quality control measurements for the excavated section. As can be seen from this table, excavated section was within the acceptable dimensions and levelness specified for the contractor.

Table 8

Control Measurements for Section's Excavation

LENGTH (ft.) (± 3 in)	90.22	90.14	91.02	90.88	91.36
WIDTH ft.) (± 3 in)	15.33	15.41	15.17	15.21	15.15
DEPTH (in) (± 0.5 in)	47-1/3	47-1/2	47-1/4	46-3/4	46-1/2
	47-1/4	47	47-1/2	47-1/4	47-1/2
LENGTH LEVELING (in.) (± 1/8 in)	1/6	1/4	1/6	1/3	1/3
	1/8	1/6	1/3	1/8	1/2
	1/6	1/8	1/4	1/2	1/3
WIDTH LEVELING (in.) (± 1/8 in)	1/4	1/4	1/8	1/6	1/2
	1/4	1/8	1/3	1/8	1/6
	1/8	1/4	1/3	1/8	1/4

Insulation and Waterproofing

Once the bottom of the excavated hole was compacted and leveled, the contractor proceeded to the installation of insulation boards. A total of 74 insulation sheets (4 ft. long by 8 ft. wide by 2 in. thick) were used to insulate the bottom and sides of the excavated hole. Duct tape was used to connect the insulation boards together (Figure 24a). The insulation sheets were also cut and adjusted based on the dimensions of the excavated pit to ensure they fit properly.

An impermeable membrane was then placed at the bottom and sides of the insulated pit. (Figure 24b). Once in place, a 2-inch layer of sand was placed (Figure 24c) on top of the impermeable membrane to protect it from being punctured by the next layer placed; that is, the filter aggregate layer.

Figure 24

Insulation and Waterproofing of Section

(a) Insulated Section

(b) Impermeable Membrane

(c) Placement of Sand

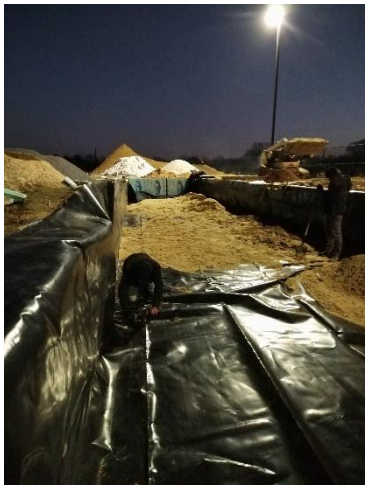

Aggregate Filter Layer and Permeable Fabric

The aggregate filter layer was then placed on top of the sand layer and was compacted in two lifts of three and four inches (Figure 25a). The material used was 3/4 inch gravel. This layer was meant to serve as a water reservoir and support the capillary

effect within the pavement structure. On top of the aggregate layer a needle-punctured polypropylene fabric was placed (Figure 25b). This fabric layer allows water to drain down into the filter aggregate layer.

Figure 25

Aggregate Filter Layer and Permeable Fabric

(a) Filter Layer

(b) Permeable Membrane

Placement and Compaction of Subgrade Layers

The contractor measured and marked the three sections in preparation for the placement and compaction of the subgrade layer in each of the test strips. As shown in Figure 26, the subgrade layers in Test Strips I and II both were constructed using Soil #2 while for Test Strip III this same layer was constructed using a one to one blend of Soils #2 and #13. The necessary materials were placed on marked locations for each strip and were graded using a grader. Figure 26a shows a picture of the subgrade layers after placement.

The subgrade layer was placed in 5 lifts (roughly 6 inches each) and each lift compacted using steel drum roller. Once all lifts were compacted, the density of subgrade layer was measured using a nuclear density gauge (Figure 26b). Table 9 presents the density measurements obtained at nine randomly selected locations for each test strip. As shown in Table 9, the field densities for the subgrade layers in each test strip varied with moisture content and soil type. Some high variations of moisture and density values can be explained by the fact that in some areas, the soils retained a higher moisture content due to rain. It is also noted that based on the recorded moisture contents, and from the proctor laboratory testing, the soils did not achieve a high compaction effort (95% of laboratory measured dry densities).

Figure 26

Placement and Compaction of Subgrade Layers in Each Test Strip

(a) Subgrade Layers Placed

(b) Nuclear Density Measurements

Table 9

Subgrade Layer Nuclear Gauge Density Measurements

Test Strip I (g/cm^3 @ % moisture)			**Test Strip II** (g/cm^3 @ % moisture)			**Test Strip III** (g/cm^3 @ % moisture)		
2.11 @ 3.7	2.14 @ 5.1	2.17 @ 3.9	2.15 @ 5.3	2.07 @ 7.5	2.15 @ 6.5	2.05 @ 7.6	2.04 @ 9.2	2.10 @ 7.2
2.16 @ 3.7	2.18 @ 4.1	2.13 @ 3.9	2.14 @ 3.9	2.15 @ 5.7	2.19 @ 6.1	2.05 @ 7.9	2.17 @ 6.0	2.10 @ 6.8
2.17 @ 5.8	2.18 @ 3.9	2.13 @ 4.1	2.13 @ 5.0	2.16 @ 5.2	2.03 @ 7.0	2.02 @ 13.2	2.11 @ 6.3	2.08 @ 7.0

Placement and Compaction of Base Layers

Once the subgrade was placed and compacted, the contractor proceeded to placing the base layer. The base layer in each strip was laid out in one lift (6 inches). The base layer in Test Strip I was constructed using DGA, in Test Strips II and III, a blend of DGA and Soil #13 (ML) (1:1 ratio) was used. Figure 27a shows the Section after placing and grading the base layer. Once in place, the base layer was compacted using a small scale drum roller (Figure 27b).

The base layer was then checked for density measurements using a Nuclear Gauge. A total of 27 measurements (9 for each strip) were performed in the same marked spots as in the case of subgrade (Figure 27c). Table 10 shows the density measurements and the corresponding moisture contents of the compacted base layers in each test strip. Although these moisture contents were under the OMC of soil samples tested in the lab, it can be seen that the field densities recorded were similar to the samples measured in lab (see Table 6).

Figure 27

Placement and Compaction of Base Layers in Each Test Strip

(a) Base Layers Placed

(b) Compaction of Base Layers

(c) Nuclear Density Measurements

To check the level of compaction for the base layers, addition Sand Cone Density Tests were performed in accordance to ASTM 1556-82, at two different locations for each test strip. Table 11 shows the averaged results of the tests performed for each strip. As seen from Table 11, the Sand Cone Density test results correlated to the Nuclear Gauge Measurements shown in Table 10.

Table 10

Base Layer Nuclear Gauge Measurements

Test Strip I (g/cm^3 @ % moisture)			**Test Strip II** (g/cm^3 @ % moisture)			**Test Strip III** (g/cm^3 @ % moisture)		
2.08 @ 4.0	2.18 @ 5.1	2.16 @ 4.1	2.14 @ 4.8	2.16 @ 7.4	2.22 @ 5.7	2.18 @ 7.0	2.11 @ 8.6	2.09 @ 7.0
2.12 @ 3.7	2.19 @ 4.3	2.13 @ 4.1.	2.14 @ 3.9	2.17 @ 5.3	2.28 @ 5.9	2.13 @ 7.4	2.16 @ 6.2	2.06 @ 7.7
2.14 @ 5.5	2.21 @ 3.6	2..11 @ 6.2	2.09 @ 4.8	2.22 @ 6.1	2.18 @ 6.2	2.00 @ 14	2.14 @ 6.3	2.03 @ 7.5

Table 11

Average Sand Cone Density Test Results

Strip No.	**Dry Density (g/cm3)**	**Moisture Content (%)**
Strip I	2.24	2.7
Strip II	2.2	4.14
Strip III	2.09	4.59

Placement and Compaction of Asphalt Layers

Placement and compaction of the asphalt layer was a month after the placement of the base layer. Since the section was built outside, it was exposed to rain and the section accumulated more moisture than desired (Figure 28a). The section was completely covered (Figure 28b) and extra time was necessary to allow water to drain to the bottom of the section from the base and subgrade layers.

Figure 28

Rain Accumulation and Covering of Section before Placement of HMA

(a) Section with rainwater

(b) Sections covered

Once water in the base and subgrade layers drained, the test strips (base layers) were compacted again and prepared for paving. The HMA layer was then placed at 3 inches thick. Due to weak soils with low bearing capacity, the paver loaded with HMA proved to be too heavy for the pavement structure and sunk in (Figure 29a). As seen from Figure 29, the HMA was placed and spread by hand using rakes. For the compaction of HMA layer, a double drum small scale vibratory compactor (Figure 29c) was used. This roller minimized rutting formation due to weak soils used as base and subgrade layers.

Figure 29

Placement and Compaction of HMA

(a) Paver stuck

(b) Placing of HMA

c) Compaction of HMA layer.

Once paved, the density of each test strips (HMA layer) was measured using a nuclear density gauge (Figure 30) at nine randomly selected locations. Table 12 shows the density measurements for all randomly selected locations per strip along with an averaged overall strip density. As can be seen from this table, the air voids exceeded 7%.The cause of high percent air voids is due to the actual paving process (manual paving) and also to the small scale compactor used to compact the HMA layer. The highest percent air voids were recorded at the edges of the section. The weakness of the

base and subgrade layer materials was also a main contributing factor towards not being able to compact the HMA layer to typical construction levels.

Figure 30

Nuclear Gauge Density Measurements

Table 12

HMA Layer Nuclear Gauge Measurements

Test Strip I (% Air Voids)			**Test Strip II** (% Air Voids)			**Test Strip III** (% Air Voids)		
21.2	21.2	13.1	9.5	10,2	10.2	10.8	9.9	9.8
10.9	10.2	14.1	11.7	10.5	13.2	10	17.9	11.7
11.3	10.3	10.7	11.2	17.7	11.4	9.9	13.7	9.8

Figure 31

Nuclear Gauge Measurements Locations and Averaged Density Values

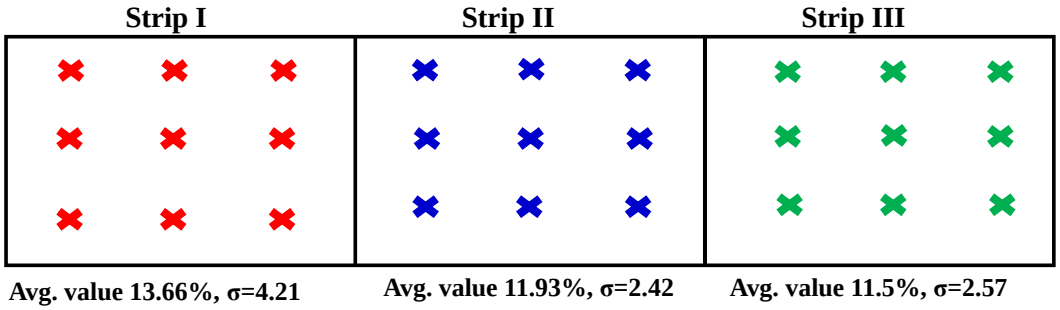

Drilling Holes for Sensor Probe and Saturation Pipes

After placing and compacting the HMA layer, the contractor proceeded to drill holes for the thermal conductivity sensors (12 in. diameter) and for the saturation pipes (4 in. diameter). As seen in Figure 31, a drilling machine mounted on a truck was used to drill the holes.

Figure 32

Drilling Holes for Sensors and Saturation Pipes

(a) Drilling Sensor Hole

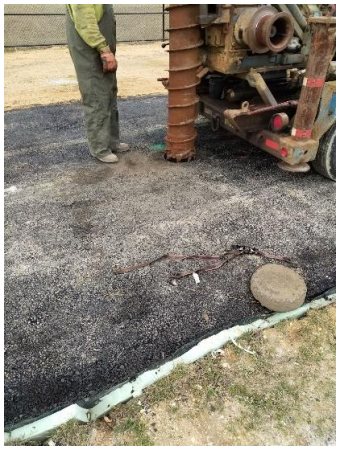

(b) Drilling Saturation Pipe Hole

Dynamic Cone Penetrometer (DCP) Testing and Results

DCP testing was performed in the drilled holes for Thermal Conductivity Sensors (TCS) and Saturation Pipes (SP) at the locations shown in Figure 32a. This test was performed in conformity with ASTM D6951 using an 8 kg hammer. In this test, an operator held the device with one hand and raised and dropped the 8 kg hammer from a set position (Figure 32b). A second person recorded the penetration value to the nearest 1 mm. The DCP was performed in order to estimate the in-situ CBR of the base and subgrade layers. The estimated CBR values at the designated locations are shown in Table 13.

As seen from Table 13, the subgrade layers for all three test strips had lower CBR values than those measured in the lab. The low field CBR values can be explained by the higher moisture content (water draining down from base layers) and also by the lower compaction levels achieved during construction. The penetration rates are inversely proportional to the CBR value. Thus, it can be observed that higher penetration rates correspond to lower CBR values.

Figure 33

DCP Testing of Test Strips

(a) Picture of DCP Device and Testing

(b) Locations of DCP Testing

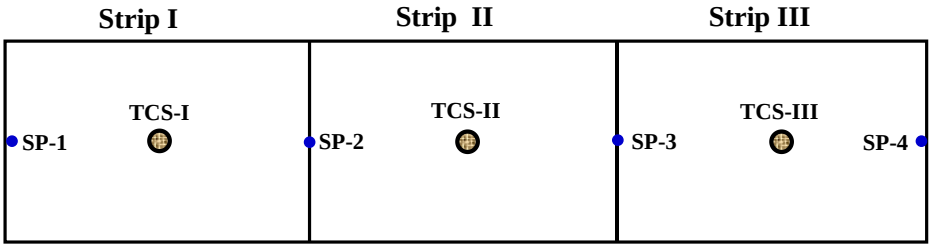

Table 13

In-Situ Calculated CBR Values for Base and Subgrade Layers[1]

Location	Penetration Ratio (mm/blow)		CBR value (%)	
	Base Layer (3-9 in. deep)	Subgrade Layer (9-36 in. deep)	Base Layer (3-9 in. deep)	Subgrade Layer (9-36 in. deep)
SP-1	22.7	119.4	8.83	1.37
SP-2	12	69.75	18.06	2.51
SP-3	12.6	46.45	17.09	3.96
SP-4	12.23	68.62	17.67	2.56
TCS-I	18	61.9	11.46	2.87
TCS-II	13.45	92.85	15.88	1.82
TCS-III	12	36.55	18.06	5.18

[1] The equation used to estimate CBR is $CBR = 292/DCP^{1.12}$ (ASTM D6951)

Instrumentation of Test Strips

The strips were instrumented with Thermal-Conductivity Sensors, a weather station and thermocouples embedded in HMA layer. All the instruments were connected to a Campbell Scientific CR1000x data logger. Additional details are provided in the following subsections.

Thermal-Conductivity Sensors

The thermal-conductivity sensors (Figure 33) were custom built by the United States Army Corps of Engineers (USACE) and were designed to penetrate the base and subgrade layer of each section. The thermal-conductivity probes had a height of 32 in. and a diameter of 12in. The probes measured in real time temperature, moisture content and thermal-conductivity of the soils they are in contact with.

Figure 34

Thermal-Conductivity Sensors

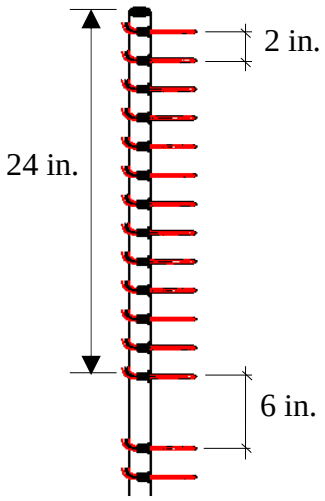

Weather Station

The weather station was installed to monitor in temperature, wind speed, solar radiation, amount of precipitation and air pressure. A ClimaVUE 50 weather station (Figure 34) was used.

Figure 35

ClimaVUE Weather Station

Thermocouples for Measuring HMA Temperature

T-type thermocouples were embedded in the HMA layer for monitoring the asphalt temperature. A total of 15 thermocouples (5 per strip) were used. Figure 35 shows the locations where the thermocouples were placed for HMA temperature monitoring.

Figure 36

Location of Embedded Thermocouples

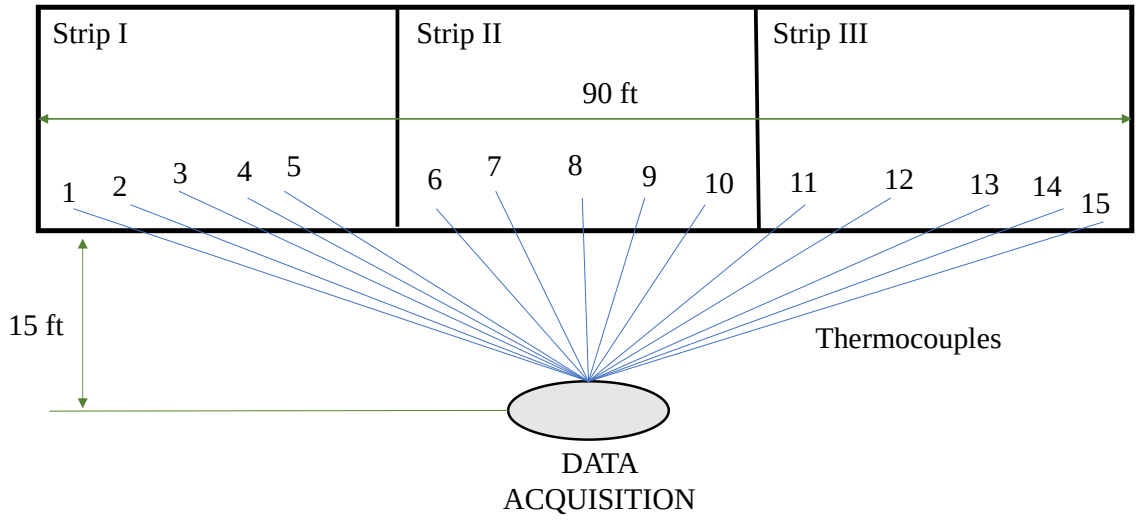

Plan for Heavy Weight Deflectometer (HWD) Testing and Monitoring of Sections

HWD Testing

HWD testing (Figure 36) was performed weekly to assess the impact of seasonal variations in moisture and temperature on the moduli values for all three layers (HMA, base, and subgrade) of each test strip. This testing was conducted at various locations in each test strip as shown in Figure 37. The data collected for HWD testing was used to back-calculate the layer moduli at different weather conditions and moisture levels.

Figure 37

Picture of HWD Used in This Study

Figure 38

Picture of HWD Used in This Study

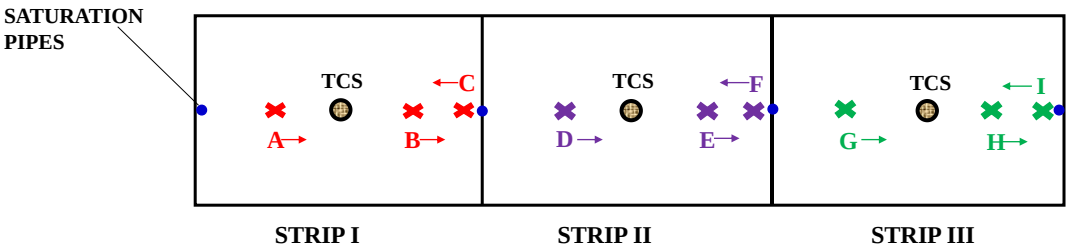

Monitoring of Moisture, Thermal Conductivity, and Temperature of Test Strips

Sensor data was monitored and recorded continuously every hour. The data included moisture of base and subgrade layers, temperatures of each of these layers at varying depths, and the thermal conductivity of these layers. This data was used to understand the changes in moisture content and thermal-conductivity within the layers (at varying depths and times of measurement). The data was also plotted, as discussed in Chapter 6, to gain an understanding of how variations in air temperature leads to changes in temperatures within the layers of each test strip.

Chapter 6

Discussion of Field Testing Results

In Chapter 6, a discussion of the HWD testing results along with analyzed sensor data is presented. Specifically, this chapter includes a discussion of the variation in moisture content and thermal-conductivity in the three test strips, the back-calculated layer moduli, and finally how changes in temperature and moisture within the sections are impacting the back-calculated layer moduli.

Temperature, Moisture, and Thermal Conductivity Variation

Temperature variations in base and subgrade layers were recorded for each day of each month (Late October 2020 through March 2021) in Test Strip I. Figure 39a, shows the average daily temperature values recorded at midpoint of both base and subgrade layers. As seen from Figure 39a, the highest internal temperature values were recorded during October 2020, while the lowest were observed during end of January and early February, 2021. The temperature values for all three layers follow the same trend. That is, the HMA layer temperatures are higher than the base and subgrade layers. That is because the HMA layer is in direct contact with the outside environment.

The subgrade layer values show a slower change (drop and rise) comparing to the base layer. That can be explained by the fact that the temperature changes at lower depth are happening at a slower pace due to heat transfer between layers. Also, it can be noticed, that the differences between the high and low temperature values for HMA and base layers are bigger than the ones inside the subgrade layer, which indicates that with depth, temperatures fluctuate less, tending to be more constant.

The moisture content change in Test Strip I layers (at mid-point of each layer) are shown Figure 39b. From this figure, the moisture contents in both base and subgrade layers were relatively similar (i.e., at ≈8.4%). Over time (October 2020 through March 2021) the moisture content also remained relatively constant (Figure 39b). The subgrade layer has shown a slightly lower (by only 0.2%) moisture content and less variation in moisture content with time. This can be explained by the type of soil used as subgrade in Test Strip I (Soil #2), which has a better water holding capacity compared to the base layer which was constructed using DGA. In addition, Figure 39b shows that precipitation (on rainy days) didn't affect the moisture inside the layers. This is believed to be due to the insulation and impermeable membranes placed when constructing the test strips.

Figure 39c, shows the thermal conductivity variations in the base and subgrade layers (at mid-point of each of these layers) in Test Strip I. As seen from Figure 39c, the base layer has shown a constant thermal conductivity overall, with some variations during October, November and December. On the other hand, the subgrade layer had a more constant thermal conductivity values during January and beginning of February, while for the rest of the other months, fluctuations can be observed. Even if small (approximately 0.1 BTU/ft.*hr*F), these spikes were recorded often, when change in moisture content was seen. Although the moisture content inside the subgrade layer was lower and more constant compared to the base layer, the thermal conductivity values of the subgrade soil (Soil #2) had a higher sensitivity to moisture changes. Thus, Soil #2 showed a higher thermal conductivity potential than the DGA material.

Figure 39d, presents the thermal conductivity as function of temperature. From Figure 39d it can be seen that the base layer had constant thermal conductivity values

comparing to the subgrade layer, where high variations were seen at different temperatures. The base layer, however shows a very small increase in the thermal conductivity values with the increase in temperature. On the other side, even though the thermal conductivity values in the subgrade layer recorded higher variations (highs and lows), the moving average tends to be constant at all temperatures. These trends are related to the type of soils used as base and subgrade layers.

The temperature variation with depth in Test Strip I is shown in Figure 40a. Averaged monthly values were used to plot the changes in temperature with depth. As seen from Figure 40a, the temperature changes from top to bottom follow the same trend (i.e., lower temperatures in the base layer than the subgrade layer). It can also be noticed from Figure 40a that with time, the temperatures drop in the test strip (all layers) due to changes in air temperatures. That can be seen from the slope changes. In March 2021, the temperatures start to increase again the section due to weather warming up in the Glassboro, NJ area.

Figure 40b shows the moisture variations with depth in Test Strip I. As seen from Figure 40b, the average monthly moisture content had a similar trend from one month to another. That is, the top of base layer and the middle and bottom of the subgrade layer show a decrease in moisture content with every month. As mentioned previously, since the section is insulated and no outside moisture infiltration occurs (other than from the top of the test strip), water drains from top layers to the bottom of the section, causing a decrease in moisture content in these layers. It is also interesting to see that at the border between the base and subgrade layers no moisture variation occurs with time. That can be explained by the fact that both, the top of subgrade layer and the bottom of base layer,

have a higher rate of compaction, which causes that specific area to hold a constant moisture content, physically allowed by the pore percentage, while still allowing the moisture flow down (the water drained is replaced by the water coming from the top of the base layer, while maintaining same moisture content).

Figure 39

Variation of Temperature, Moisture Content, and Thermal Conductivity in Test Strip I (Values at Mid-Point of Layer)

(a) Temperature Variation

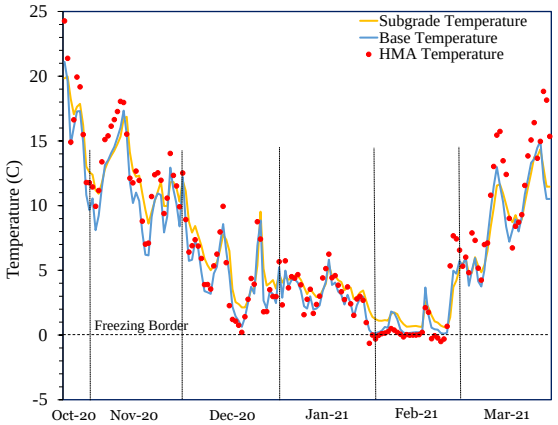

(b) Moisture Variation

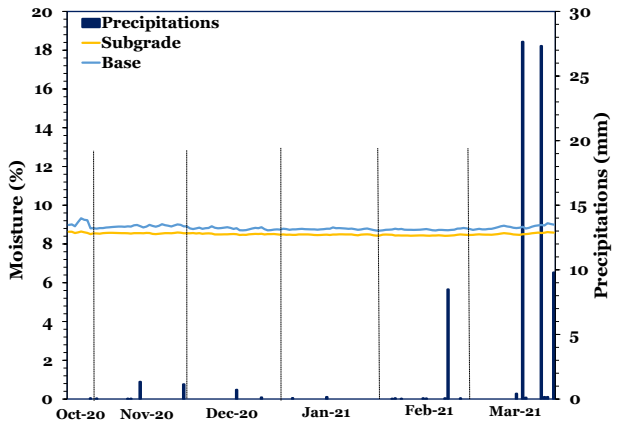

(c) Thermal Conductivity and Moisture Variation

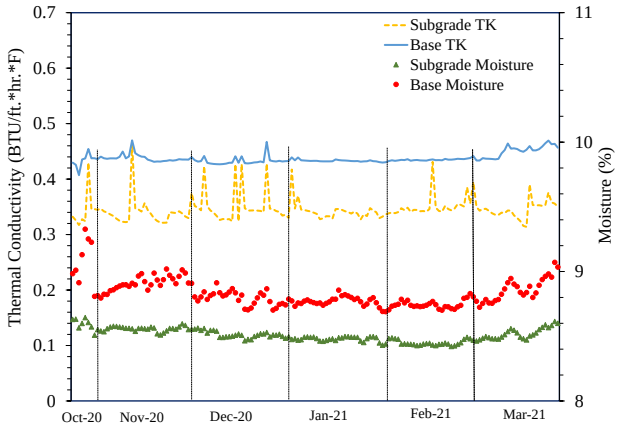

(d) Thermal Conductivity vs. Temperature

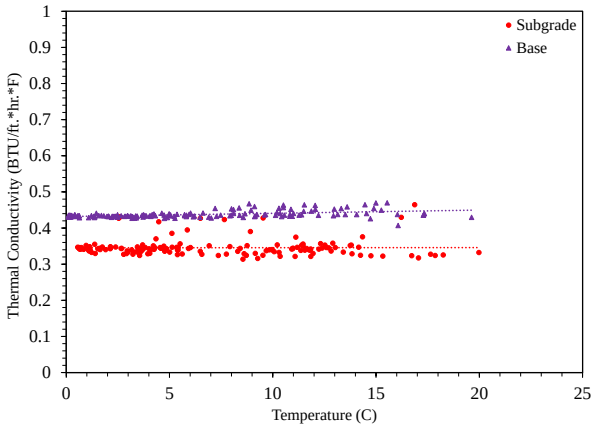

Figure 40

Variation of Temperature, Moisture Content, and Thermal Conductivity with Depth

(a) Temperature vs. Depth

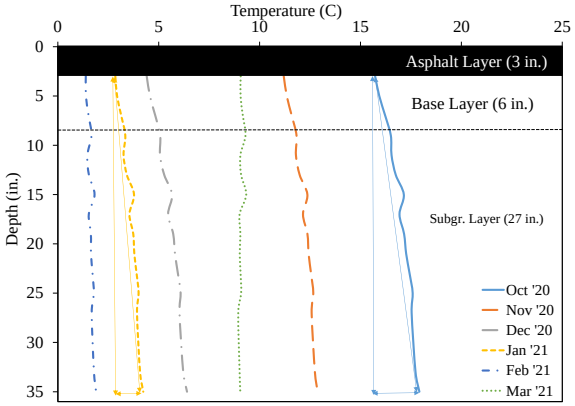

(b) Moisture Content vs. Depth

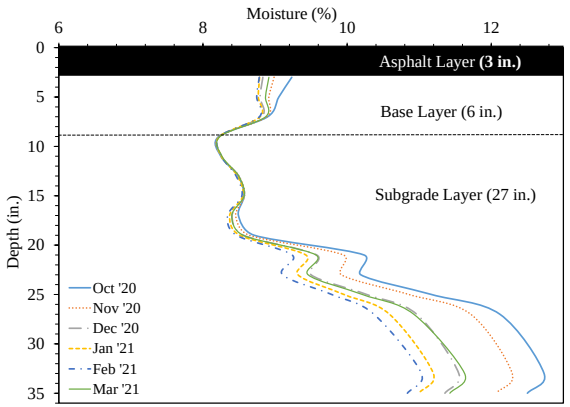

(c) Thermal Conductivity vs. Depth

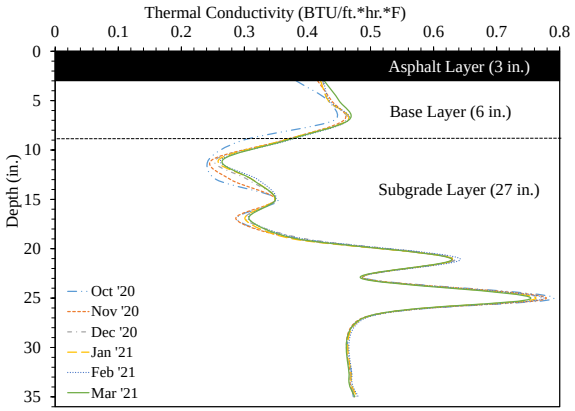

The thermal-conductivity variations with depth are shown in Figure 40c for Test Strip I. The average monthly thermal-conductivity values follow the same trend with depth for all months considered in this study. From Figure 40c, it can be seen that the base and top of the subgrade layers, are showing slight variations in thermal-conductivity values. The rest of the subgrade layer, however, maintains relatively constant thermal-conductivity levels for all months. The thermal conductivity values follow the moisture trend (see Figure 39b), with higher values at the bottom of the subgrade layer. The constant thermal conductivity values with time inside the subgrade layer can be explained by the small moisture variations from one month to another in this portion of the subgrade.

HWD Measured Deflections

Figures 41 through 43 present the HWD measured deflections for Test Strips I, II, and III on select days. Figure 41 presents those deflections for Strip I. As can be seen from this figure, HWD deflections measured for Test Strip I from sensor one (immediately under load) were around 40 to 60 mils in December, decreased to around 40 mils in January, then increased to the 40-60 mils range in February, and in March these deflections decreased slightly to the lower 40s mils range. Figure 41 also shows minimal variation in deflections measured in the sensors farther away (sensors four through seven) from the loading spot, regardless of the time when the data was collected (or in other words the air temperature). This indicates that most of the variation (potentially due to materials and compaction) in this test strip in mainly in the upper layers. It can also be seen from Figure 41, regardless of testing day, that test location A

had higher deflections those measured from locations B and C. The cause of high deflections at this location is mainly because Point A was an edge point in Test Strip I. This point also, since it is close to the section entrance created by the contractor, had lower levels of compaction during construction.

The measured HWD deflections for Test Strip II are shown in Figure 42. Similar to the trend observed in Test Strip I, Figure 42 shows that deflection Strip II were higher in December, then decreased in January, then increased again in February and finally remained relatively similar in March. The measured de-flections in this test strip measured under the applied load (sensor one) also varied from 40 to 64 mils depending on test day and location. Figure 42 also shows that variation in the measured deflections is mainly in sensors one through three and that sensors four through seven recorded relatively similar deflection measurements. This again suggests that most of the variation in this section is mainly in the upper layers and in particular in the HMA layer. Similar observations/trends can be seen from the deflections measured for Test Strip III (Figure 43). However, it is noted that Position I is again an edge position; thus, explaining the higher variability in measured deflections at this location than the other two (G and H).

By comparing the deflections measured for all three test strips (Figure 41 through 43), valuable information can be inferred about how the structural integrity of the strips (i.e., higher deflections usually mean less stability than lower deflections). To facilitate this comparison, only the March 2021 deflections for all test strips are discussed here but similar conclusions can be drawn from other testing days. From Figures 41d, 42d, and 43d, it can be seen that Test Strip I had deflections in the upper 40s mils, Test Strip II had

deflections in 40 to 60 mils range, and Test Strip III had deflections ranging between 36 and 62 mils. All these values are from sensor one (immediately under load). These values suggest that all test strips have similar structure integrity (in HMA layer) with Test Strip III being the most variable of all three strips. This was expected because test Strip III was constructed using a modified base and subgrade materials (blends of DGA and Soil #13, Soil #2 and Soil #13). Similarly, when evaluating deflections from other sensors (e.g., sensors three through seven), it can be seen that all test strips had similar measured deflections indicating that the lower layers were consist (that is, similar compaction levels applied and similar integrity) throughout.

Impact of Moisture and Temperature on Back Calculated Layer Moduli

The stiffness of each layer of the pavement section was back calculated using BAKFAA, a software developed by the Federal Aviation Administration (FAA). BAKFAA computes theoretical deflections by matching the radius of curvature of the measured and calculated deflection basins, which ensures that more representative elastic moduli values are outputted.

Since the section was designed to use frost-susceptible weak soils, the back calculated values for the modulus for all layers were not in the typical ranges.

Figure 44 shows the back calculated stiffness and its variation with time for all test strips. As seen in Figure 44a, the back-calculated moduli values for the HMA layer in Test Strip I ranged between 300 to 500 ksi with one measurements reaching up to 560 ksi (late January, temperature? at a recorded HMA temperature of 2.8°C). The base layer

(DGA in Strip I) had a layer modulus values ranging 100 to 200 ksi while the subgrade layer (Figure 44a) had varying subgrades in the range of 1-2 ksi. Compared to typical pavement structures, these layer moduli values for all layers are weaker than typical. This was expected due to the construction materials used for Strip I (and all other strips for that matter) were not suitable for paving applications (highly frost susceptible).

Figure 44b shows the back calculated moduli values with time for Test Strip II. As shown in this figure, the HMA layer had range of 250 to 450 ksi moduli values, the base layer (DGA) had layer moduli values ranging from 100 to 200 ksi, while the subgrade, similar to Strip I, showing low layer moduli values (ranging between 1 to 2 ksi). A similar trend in layers moduli values can also be observed for Strip III (Figure 44c). The difference; however, between this test strip and other two is that Strip III showed more variability in back-calculated moduli values for all layers.

In addition, by comparing the layer moduli for all three strips, it can be seen that Strip I seem to be the strongest of all three strips. This was expected because the materials used for construction this strip was the "best" with HMA at the top, unmodified DGA as base layer, and Soil #2 as the subgrade layers. Strip II had slightly lower layer moduli values than Strip I indicating that it is slightly weaker. This can be explained by the use of a modified base materials (blend of DGA and Soil #13). The higher variability in Strip III is also mainly attributed to the different blends of materials used for the base and subgrade layers.

Figure 41

Heavy Weight Deflectometer (HWD) Deflections Measured for Test Strip I

(a) December 24, 2020

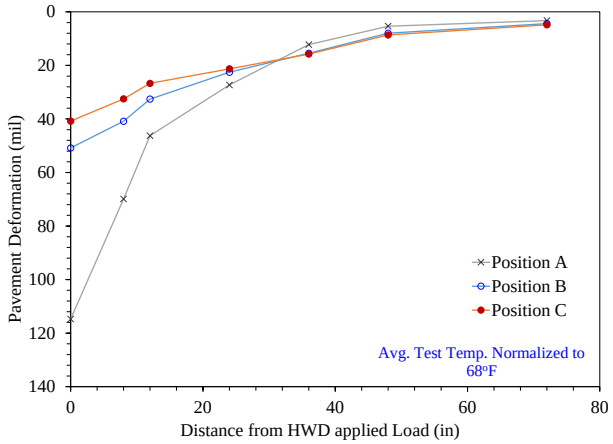

(b) January 22, 2021

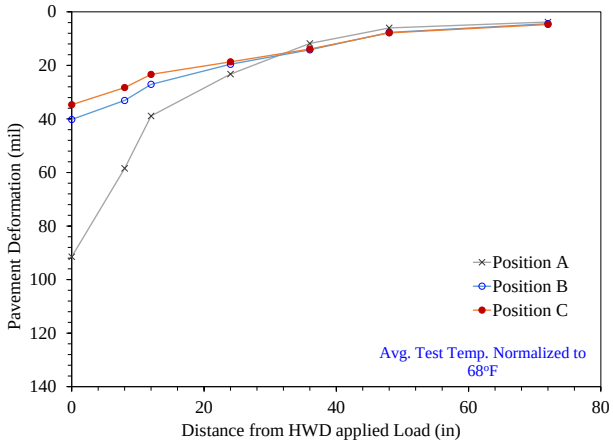

(c) February 22, 2021

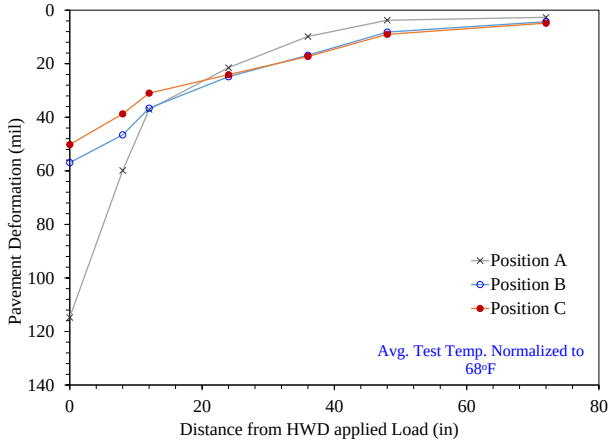

(d) March 25, 2021

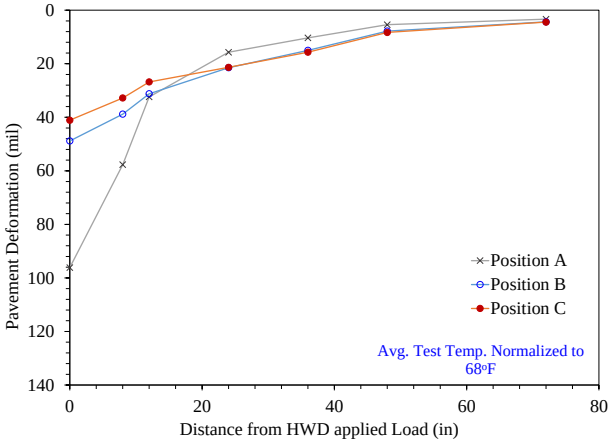

Figure 42

Heavy Weight Deflectometer (HWD) Deflections Measured for Test Strip II

(a) December 24, 2020

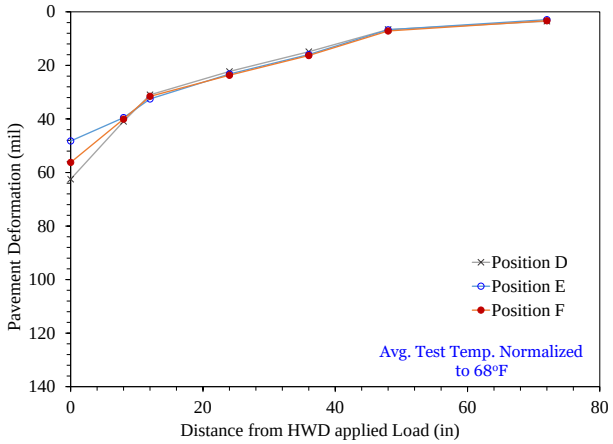

(b) January 22, 2021

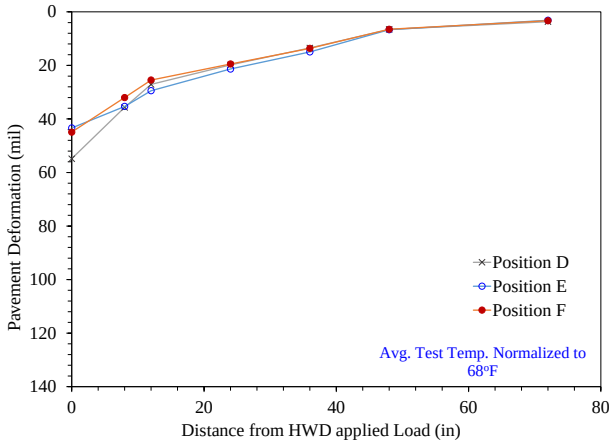

(c) February 22, 2021

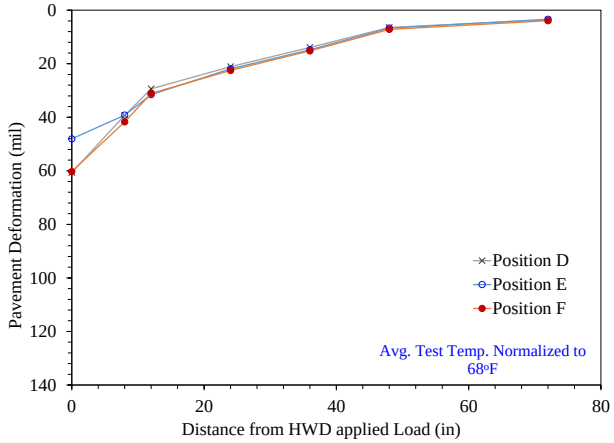

(d) March 25, 2021

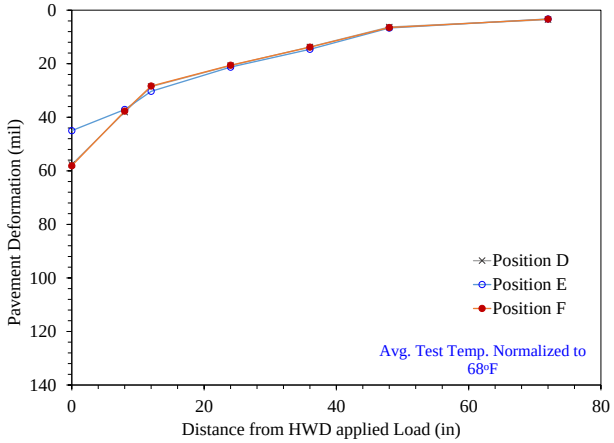

Figure 43

Heavy Weight Deflectometer (HWD) Deflections Measured for Test Strip III

(a) December 24, 2020

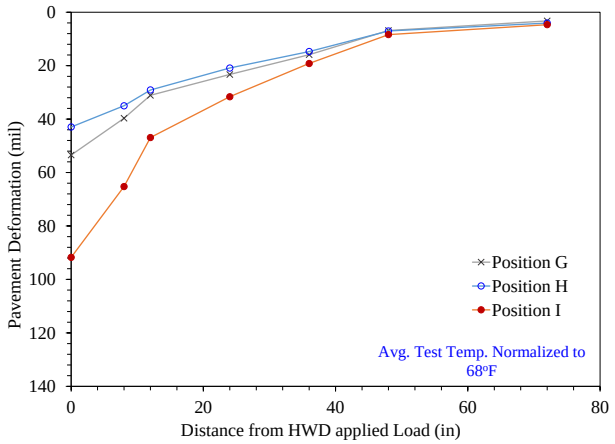

(b) January 22, 2021

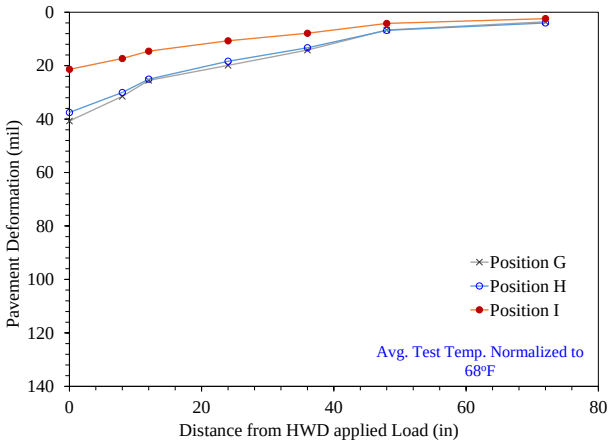

(c) February 24, 2021

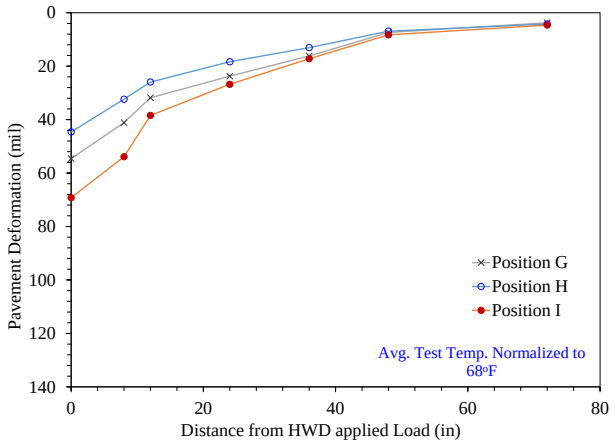

(d) March 25, 2021

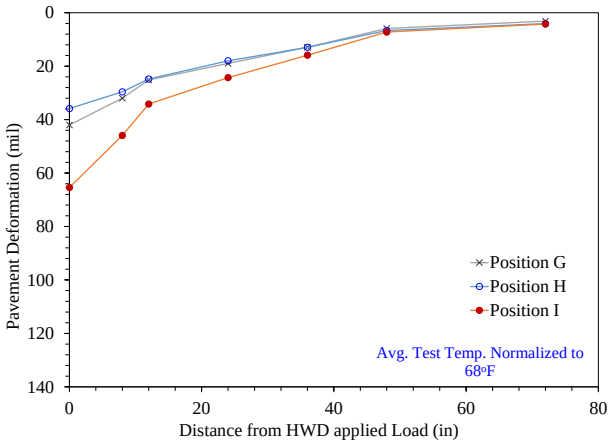

Figure 44

Variation of Back Calculated Stiffness with Time

(a) Strip I

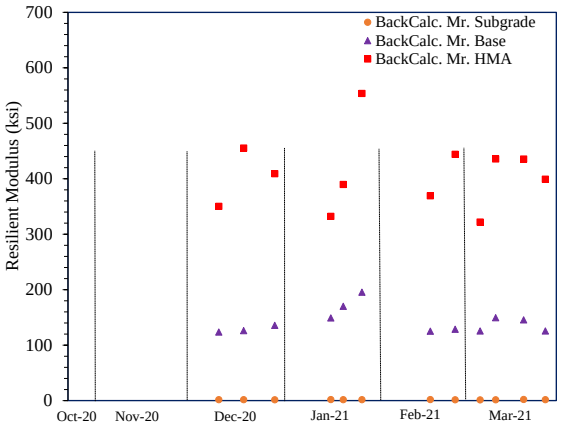

(b) Strip II

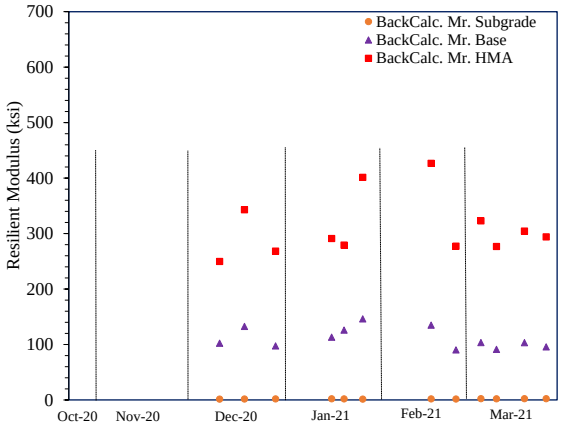

(c) Strip III

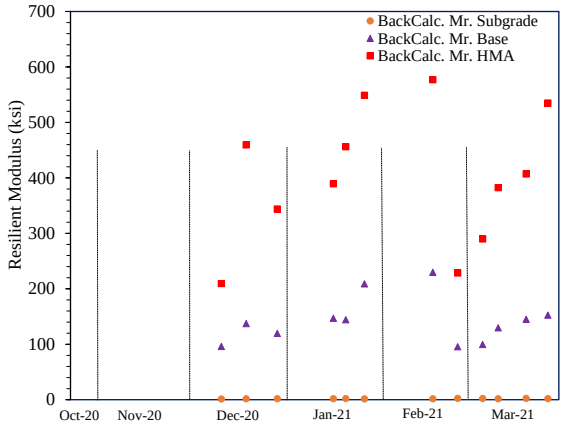

Chapter 7

Summary, Conclusions and Recommendations

Summary

In this project, a comprehensive laboratory testing plan was conducted to select two frost-susceptible soils for use in constructing three full-scale test strips. A total of 16 soils were obtained from various suppliers in NJ and were evaluated determine their frost-susceptibility. The evaluation included conducting sieve analysis, hydrometer analysis, and specific gravity. Using these measures, two soils were selected (namely, Soil #2 and Soil #13) for constructing the test strips. The properties (Atterberg Limits, moisture-density relationships, California Bearing Ratio (CBR), among others) were determined through a laboratory testing plan.

In addition, this study involved constructing three full-scale test strips (in one section) at the CREATEs full-scale testing facility. The first test strip was constructed using a typical NJ HMA mix, a typical dense graded aggregate base (DGA), and Soil #2 used as the subgrade. Test Strip II was constructed using the same HMA mix, a blend of DGA and Soil #13 (one to one), and Soil #2 as the subgrade layer. Test Strip III had a blend of DGA and Soil #13 for the base layer and a one-to-one blend of Soils #2 and #13 for the subgrade layer. All three test strips were evaluated using the HWD on weekly basis. Test Strip I also included a thermal conductivity probe that is capable of measuring moisture content, temperature, and thermal conductivity at varying depths in the base and subgrade layers.

Summary of Findings

The following findings of laboratory work were highlighted:

- Both soils (#2 and #13) contained high amounts of fine particles. Soil #13 showed a 58% particles passing Sieve No. 200 sieve and had a considerably higher amount of fine particles than Soil #2 (24%).
- Soils #2 and #13 had a low Plasticity Index values (PI < 7). While Soil #2 had PI of 4.57%, Soil #13 showed a slightly lower PI of 1.45%.
- Soil #2 had a Maximum Dry Density (MDD) of 2.08 g/cm^3, while Soil #13 proved to be less dense, with a MDD of 1.73 g/cm^3. On the other side, Soil #13 had a higher Optimum Moisture Content (OMC) than Soil #2. If Soil #13 recorded 17.1% OMC, Soil #2 had a decreased value of 11.61%.
- Both soils showed very low CBR values. Soil #2 had a CBR value of 7.1%, while the CBR value for Soil #13 proved to be slightly higher at 7.8%.
- While Soil #2 (SC) showed a low Resilient Modulus value (50 MPa), M_r was not measured for Soil #13 (ML) due to failure of samples during testing. An M_r value was estimated for Soil #13 (65 MPa) using an empirical relationship with CBR results.

Based on the HWD testing and analyzed sensor data, the findings were:

- The temperature in Test Strip I for all three layers (HMA, base, and subgrade) followed the same trend. The differences in temperature between these three layers were at most 4°C.

- The moisture contents in both base and subgrade layers of Strip I were relatively similar (i.e., at ≈8.4%). Over time (October 2020 through March 2021) the moisture content also remained relatively constant. The subgrade layer has shown a slightly lower (by only 0.2%) moisture content and less variation in moisture content with time.
- The base layer (Strip I) has shown a constant thermal conductivity trend, with some variations during October, November and December. The subgrade layer; however, had a more constant thermal conductivity values during January and beginning of February, while for the rest of the other months, fluctuations can be observed. Even if small (approximately 0.1 BTU/ft*hr*F), these spikes were recorded often, when change in moisture content was seen. Although the moisture content inside the subgrade layer was lower and more constant compared to the base layer, the thermal conductivity values of the subgrade soil (Soil #2) had a higher sensitivity to moisture changes.
- Minimal variation in deflections (2-12 mils) were measured in the sensors farther away (sensors four through seven) from the loading spot, regardless of the time when the data was collected (or in other words the air temperature) or the test strip being considered.
- Test Strip III was the most variable from among all three test strips. In terms of back calculated moduli, Strip III recorded values between 230-580 ksi for the HMA layer during the February month, when the recorded temperature difference was only 3°C.

- The back calculated moduli values show that Test Strip I had the highest structural integrity (i.e., high and least variable moduli values) of all three strips. The highest difference between back calculated moduli values for the HMA layer was observed in January month (335-555 ksi, corresponding to temperature values of 5.1°C, and 2.8°C). As for the base layer, for the same month the calculated moduli values varied between 150 ksi (at 4.1°C) and 195 ksi (at 2.3°C).

Conclusions

Based on the summary of findings, the following conclusions were drawn:

- Both soils are frost-susceptible. The percent of fine particles and type of soil determined as result of gradation and Atterberg limits testing, proved that the soils have frost-susceptible potential. Based on Frost Susceptibility Classification (USACE, 1984), it was found that Soil #2 can be classified as F3(b) frost-susceptible soils, while Soil #13 is classified as F4(a) frost-susceptible soils.
- Based on Atterberg limits testing results, both soils (#2 and #13) are low plastic (PI<7). The low plasticity of these soils correlates to a low clay content, thus a lower water holding capacity and a lower frost-susceptibility potential. Low clay content is also associated with low cohesion between soil particles.
- Soil #2 it is more compactible (higher MDD), while Soil #13 may have a higher permeability. Since Soil #2 can achieve higher density under compaction, based on the goals of this study, it was used as subgrade and a compaction rate of 80-85% was targeted for a larger number of voids, thus a better water retention

capacity. Soil #13 was used in a blend with DGA as base layer, for which, a minimum of 95% compaction was targeted.

- Both soils have a low bearing capacity. Since CBR is a measure of strength of materials, based on CBR values, both soils are considered weak and unsuitable as base and subgrade layers. Low CBR values were obtained because of the large amount of fine particles in these soils. However, the purpose of the study was using frost-susceptible (weak) soils.
- The estimated and measured M_r values indicate that both soils are weak. Low resilient modulus values obtained form laboratory testing are typical for these types of soils. Low resilient modulus values are associated with the inability of these soils to resist traffic loads. Since the section was designed to be weak, the Heavy Weight Deflectometer (HWD) testing was performed using the smallest weight available so no high deformations occur.
- Temperature variations of HMA, base and subgrade layers followed the same trend during October through March months. This indicates that the sensors provided veridical and consistent data. The temperature recorded by the sensors had the same variations throughout the depth of the section. As expected, there were differences between the temperature values of layers. The HMA layer had the highest temperature since it was in direct contact with the outside environment.
- The temperature changes at lower depth are happening at a slower pace due to heat transfer between layers. More rapid changes in temperature values were seen in the upper layers. Since the lower layers are located further away from the

outside environment, the changes in temperatures were happening slower, with the tendency to be more constant. This is explained by the slower heat transfer between layers and also by the type of material and moisture content inside the layers.

- Moisture contents in both, base and subgrade layers, remained relatively constant from October through March. This proves the efficacy of insulation of the sections since no underground water entered the section. Also, since moisture within layers didn't change, the precipitations didn't have any impact on the moisture inside the section. Also, the constant moisture values are distributed by thicknesses of layers, with higher (but constant) values in the lower subgrade, due to gravitational movement of the water.
- SC soil (Soil #2 used as subgrade for Strip I) showed a higher thermal conductivity potential than DGA (used as base for Strip I). The higher thermal conductivity potential is explained by the high fluctuations in thermal conductivity values with small changes in moisture content. Soil #2 also had a higher clay content, thus a better water retention potential. Higher water retention potential correlates with higher thermal conductivity.
- Most of the variation in deflections in all test strips is mainly in the upper layers. This is explained by the weak (high air voids) HMA layer resulted from ununiform placement (paved by hand) and compaction (small scale compactor), and also indicates that the subgrade layers for all three strips are very weak. The variation in deflections for the upper layers in all three strips is explained by the fact that all strips have similar structural integrity.

- Highest variability in deflections were recorded for Strip III. The variability in deflection is explained by the variability of materials, since Strip III was constructed using blends of materials used in Strip I and Strip II. The materials used were very weak and had low resilient modulus values.
- Strip I had the highest structural integrity (i.e., high and least variable moduli values) since it was constructed with typical paving materials (i.e., HMA surface course and DGA base layer) and Soil #2 as subgrade layer.

Recommendations

This research focused on finding the impact of temperature, moisture and thermal conductivity variations on structural capacity of a pavement section divided in three strips, with different frost-susceptible layers. The data collected will be used by CRREL to validate the FROST Model.

This study was conducted from October through March, without achieving sub-freezing temperatures inside the pavement's layers. For future, for a more comprehensive study and wider range of data collection, the following are recommended:

- Conduct temperature controlled testing. Using a cooling unit with a freezing panel placed on top of the section, can help freeze the sections in a controlled manner and collect data from frozen layers.
- Conduct HWD testing on frozen section and analyze deflections of all different frost susceptible base and subgrade layers.

- Expose the section to repeated freeze-thaw cycles and determine moisture and thermal conductivity movements within frost susceptible layers.
- Measure frost depths in all three strips and compare it to the values determined by using different frost prediction models.

References

Andersland O., & Ladanyi, B. (2004). *Frozen Ground Engineering (Second Edition).*

Bianchini, A., & Gonzalez, C. R. (2012). *Pavement-transportation computer assisted structural engineering (PCASE) implementation of the modified Berggren (ModBerg) equation for computing the frost penetration depth within pavement structures.*

Casagrande, A. (1931). *Discussion on frost heaving.* Paper presented at the Proceedings, Highway Research Board.

Chamberlain, E. J. (1981). *Frost susceptibility of soil, review of index tests.*

Deen, R. C. (1964). *Frost penetration into a multi-layered soil-water system. (Ph.D.).* Purdue University.

Edgers, L., Bedingfield, L., & Bono, N. (1988). *Field evaluation of criteria for frost susceptibility of soils.* Transportation Research Record, 1190, 73-85.

Gandahl, R. (1987). *Frost and Frost damage*. VTI Report no. 546. Linkoping, Swedish Road and Traffic Research Institute, Sweden.

Guymon, G. L., Berg, R. L., & Hromadka, T. V. (1993). *Mathematical model of frost heave and thaw settlement in pavements.*

Haley, J. F. (1963). *Frost Considerations in Highway Pavement Design.* Eastern United States Highway Research Record (33).

Janoo, V.C., Berg, R.L. (1990). *Thaw weakening of pavement structures in seasonal frost areas.* Transp. Res. Rec. 1286, 1990.

Johnson, A. (2012). *Freeze-thaw performance of pavement foundation materials.* (Master of Science), Iowa State University.

Johnson, T. C. (1978). *Design of Civil Airfield Pavements for Seasonal Frost and Permafrost Conditions.* Transportation Research Board Special Report(175).

Konrad, J.-M. (1999). *Frost susceptibility related to soil index properties.* Canadian Geotechnical Journal, 36(3), 403-417.

Lambe, T. W. (1956). *Modification of frost-heaving of soils with additives.* Highway Research Board Bulletin (135).

Lein, W. (2019). *Frost-Depth Penetration and Frost Heave in Frost-Susceptible Soils.* ERDC/CRREL TR-19-24.

McHattie, R., Connor, B., Esch, D. (1980). *Pavement structure evaluation of Alaskan Highways.* Research Report FHWA-AKRD-80-1. Alaska Department of Transportation and Public Facilities.

National Asphalt Pavement Association (NAPA), (1994). *Guidelines for Use of HMA Overlays to Rehabilitate PCC Pavements.* Information Series 117.

Nordal, R.S., Hansen E., (1982). *Detection and prediction of seasonal changes of the bearing capacity at the Vormsund test road.* Proceedings of the International Symposium on Bearing Capacity of Roads and Airfields, 23–25 June, Trondheim, Norway. Norwegian Institute of
Technology. Tapir Publishing, Trondheim, pp. 374–382.

Penner, E. (1959). *The mechanism of frost heaving in soils.* Highway Research Board Bulletin (225).

Popik, M., & Olidis, C. (2005). *The effect of seasonal variations on the resilient modulus of unbound materials.* Annual Conference of the Transportation Association of Canada.

Powell, W., Potter J. (1984). *Transportation and Road Research Laboratory (TRRL) Report LR. pp. 62, 1132.*

Rajaei, P., & Baladi, G. Y. (2015). *Frost Depth: General Prediction Model.* Transportation Research Record: Journal of the Transportation Research Board (2510), 74-80.

Simonsen, E., & Isacsson, U. (1999). *Thaw weakening of pavement structures in cold regions.* Division of Highway Engineering. Royal Institute of Technology. SE-100 44 Stockholm, Sweden.

Sowers, G. (1979). *Introductory Soil Mechanics and Foundations Geotechnical Engineering.*

Taber, S. (1929*). Frost heaving.* The Journal of Geology, 37(5), 428-461.

Turner, K. A., & Jumikis, A. R. (1956). *Loss of bearing capacity and vertical displacements of New Jersey soils. Ground Freezing, 24.*

USACE. (1984). EM 1110-3-138, 1984. *Pavement criteria for seasonal frost conditions — mobilization construction.* Engineer Manual. Washington, D.C., USA: Department of the Army Corps of Engineers.

Yoder, E. J., & Witczak, M. W. (1975). *Principles of pavement design: John Wiley & Sons.*

Zhang, W., & Macdonald, R. A. (2003). *The Effect of Freeze -Thaw Periods on a Test Pavement - in the Danish Road-Testing Machine.*